Vortex interactions between a pair of bubbles rising side by side in ordinary viscous liquids

Jie Zhang,[1,*] Long Chen,[2,*] and Ming-Jiu Ni[1,2,†]

[1]*State Key Laboratory for Strength and Vibration of Mechanical Structures, School of Aerospace, Xi'an Jiaotong University, Xi'an 710049, China*

[2]*School of Engineering Science, University of Chinese Academy of Sciences, Beijing 101408, China*

(Received 5 April 2018; published 30 April 2019)

We report on a series of numerical results about a pair of bubbles rising side by side in various silicone oils, with the terminal Reynolds number to vary between 10 and 700 and the aspect ratio of the bubble shapes to vary between 1.0 and 3.2. Through fully solving the three-dimensional Navier-Stokes equations, different interactive behaviors between the two bubbles are reproduced, such as the repelling, the attracting coalescence, the attracting bounce, and the repeated bounce, which are also observed in the experiments. First, we determine that, if there are no toroidal vortex rings attached at the rear end of the bubbles, the moderate- to high-Reynolds-number bubbles tend to attract with one another after being released, and, subsequently, whether they will coalesce or bounce after contact depends on the development of the vortex structures. In contrast, if toroidal vortex rings are generated in the bubble wake in other parameter spaces, a pair of bubbles will repel one another after being released, and a subsequent repeated bounce will be even observed. Lastly, an available force calculation model enables us to identify the relation between the forces and the vorticity produced on the bubbles when the pair of bubbles collide.

DOI: 10.1103/PhysRevFluids.4.043604

I. INTRODUCTION

Bubbly flows are commonly encountered in many industrial applications, such as in heat exchangers and the metallurgy industry, where bubbles are generated or injected into the reactors for heat and mass transfer enhancement. Therein, the structures of the flow field considerably depend on the bubble volume fraction, the bubble distribution, and the bubble interactions. Therefore, in order to predict the evolution of the flow field, it would be necessary to understand the dynamic behaviors when the bubbles interact with each other during their motion. However, as far as the authors know, the understanding of such bubbly flows is far from satisfactory, particularly with regard to the underlying mechanisms that cause even a pair of bubbles to interact with each other.

Because the interactions between the bubbles are complicated inside the bubbly plumes, most of the theoretical studies in the past [1,2] considered the flow to be irrotational due to the high Reynolds number, thus obtaining a formation of horizontal bubble clusters. However, this result was not consistent with the experimental observations [3], in which the bubbles were observed to be distributed homogeneously. Therefore, the vortex effects and the bubble deformations are worthy of attention in studying such bubbly flows.

Alternatively, the case of two bubbles rising in line is the most simplified case that has been studied in the recent years. By employing the potential flow model, Kok [4] found that two spherical

*These authors contributed equally to this work.

†mjni@ucas.ac.cn

bubbles would attract each other when the angle between their centerlines and the direction of motion was in the range of $[\theta_{cr}, 180^\circ]$, whereas θ_{cr} was the critical angle ranging from 35° to 54.7°; otherwise, the bubbles would repel from one another. Harper [5] obtained similar results by supposing the flow to be irrotational. However, through direct numerical simulations [6], the influence of the bubble wake was found to be important enough that the bubbles in line would attract (repel) one another when Re was small (high). Based on this, Harper [7] then revised his theoretic model by adding the vortical effect, and the new results were consistent with the numerical solutions. Recently, Sanada *et al.* [8] conducted a series of experiments about a pair of bubbles rising in line; they confirmed there to be a critical Re to determine whether the lower bubble would catch up or stay away from the upper bubble. Moreover, they also observed an interesting phenomena that the lower bubble would escape from the rising line in some cases, which might be also attributed to the wake effect behind the upper bubble.

When the pair of bubbles are rising side by side, Legendre and Magnaudet [9] performed direct numerical simulations by keeping the bubbles with frozen spherical shape. They showed that when Re was larger than a critical value Re_{cr}, which depended on the distance between the bubble centroid, the pair of bubbles were attracted with one another due to the Venturi effect. However, when $\mathrm{Re} < \mathrm{Re}_{cr}$, the vorticity produced around each bubble would interact and a blocking effect was generated to repel them. Furthermore, Hallez and Legendre [10] extended this model to more general cases while the positions of the two bubbles were arbitrarily arranged. Besides the Re_{cr}, they also found a critical angle θ_{cr} to determine whether the two bubbles would attract or repel each other, as Kok [4] obtained theoretically. However, as validated in the recent numerical simulations [11,12], the three-dimensional double-threaded vortex structures would not emerge behind a spherical bubble regardless of Re. Therefore, the influence of the bubble deformation and the wake instability were not considered in their works. Duineveld [13] conducted a series of experiments about two bubbles rising side by side in the pure water, whereas the bubble deformations were significant. He found that the bubbles would always attract each other first, but bifurcations emerge when they got closer: Coalescence happened between small bubbles ($R < 0.71$ mm, where R is the bubble radius) while bounce was observed between large bubbles($R > 0.71$ mm). He concluded that there existed a critical Weber number (We, hereafter), which was based on the horizontal approaching velocity of the pair of bubbles, for the criteria of coalescence or bounce. He conjectured the bubble bounce was caused by the shedding of vortices, but it was not observed or verified. More recently, Sanada *et al.* [14] performed more sophisticated experiments by employing the water and various silicon oils as working fluids, whereas different interactions between the pair of bubbles were observed, such as repelling, coalescence, and bounce. Nevertheless, they thought the critical We was based on the rising velocity, rather than the bouncing velocity, as Duineveld gave. Moreover, the wake interactions behind the bubbles were observed in their experiments, proving that the collision between two bubbles was related to the vortex structures. However, detailed discussion about this mechanisms was not given due to the limitations in experimental measurements.

In addition, in the case of the single bubble motion, the wake instability has been widely admitted as the cause of path instability. It has been found that the bubble will perform a zigzag motion in pure water when the bubble size is larger than $R = 0.91$ mm [15,16]. Then, many experimental investigations have been devoted to the cause of the path instability, which can be found in different works [17–19]. However, until Mougin and Magnaudet [20] presented the numerical observations of the wake patterns behind the ellipsoidal bubble, it was confirmed that the path instability was ascribed to the wake instability when the generated vorticity on the bubbles surface could not be evacuated away by the flow. This observation was further verified by Shew and Pinton [21] by applying a Kirchhoff's equation to predict the forces on bubbles, and they interpreted that the formed wake structure was very similar to the trailing vorticies on an airplane wing. To further understand the transition process of wake instability, Magnaudet and Mougin [11] studied the evolution process of the flow past a fixed ellipsoidal bubble; they obtained the threshold for the wake instability by changing Re and the aspect ratio χ, and the transition curve was obtained. By applying a linear stability analysis, Yang and Prosperetti [22]) observed similar results: The formation of

the double-threaded wake would cause the bubble to deviate from the straight trajectory. More recently, Cano-Lozano *et al.* [23] gave a phase diagram to identify the parameter spaces for different rising behaviors of the single bubble, and they confirmed the wake structures would be distinctive with respect to different rising paths. Based on this, our latest study [24] gave an interpretation about the mechanisms causing the bubble to transit from zigzag to spiral, further stressing the importance of the vortex types in inducing different bubble rising paths. To sum up, the wake structures behind the bubble are decisive in controlling the rising behaviors of the bubble motion. As a consequence, we also have reasons to believe that it is actually the wake structure rather than the collision velocity to determine the interactions between the pair of bubbles; moreover, the developments of the vortical structures also depend on various flow conditions, such as the fluid properties, the bubble sizes, and the separated distance between the pair of bubbles. In addition, another respect requires attention: When the path instability happens on the single bubble motion, the double-threaded vortex structures are generated. Sometimes it is because of the breaking of the axisymmetric vortex ring behind the bubble, but sometimes it is not. Therefore, whether there are such standing eddies attached at the rear of the bubble is also very important during the interactions between the pair of bubbles.

With the open source code GERRIS, developed by Popinet [25], the freely rising pair of bubbles are simulated in the present study numerically by adopting the volume-of-fluid (VOF, hereafter) tracking method, we focus on the physical mechanisms causing different interactive behaviors between the two bubbles, and we catalog the interactions into four patterns: (1) repel with one another, (2) coalesce after attracting, (3) bounce after attracting, and (4) repeated bounce. In this paper, different vortex structures in the four cases are presented respectively, and then we prove that the development of the vortex structures plays a crucial role in the bubble interactions, and more importantly, one of the main focuses in the present study is to clarify that the interactive behaviors between the pair of bubbles also depends on whether there are toroidal vortex rings generated at the rear of the bubble before they collide because such vortex structures only appeared within limited parameter spaces [12]. Otherwise, during the preparation of this paper, we noticed that there was a similar paper published by Tripathi *et al.* [26], who also used GERRIS to simulate the interactions between the pair of bubbles. However, their study just focused on the repeated-bounce interactions, for which the toroidal vortex rings were always attached behind the bubbles within their investigated parameter spaces, but it was not indicated very clearly in that paper.

This paper is organized in the following manner. Section II states the problem and describes the interactive behaviors between a pair of bubbles rising side by side. Section III describes the numerical methods, validations, and overview of the numerical results about different bubble interactions. In Secs. IV and V, 15 numerical results are presented and we show that the bubble interactions are relevant to the wake vortices formed behind the bubble, while their evolutions in differen flow conditions are also presented. Section VI discusses the rising velocity and the forces experienced by the bubble when the interactive behaviors between the pair of bubbles are varied. Finally, the conclusion is drawn in Sec. VII.

II. PHYSICAL MODEL

A pair of spherical bubbles, with equal size of D in diameter and with an initial separated distance of S, are released freely at the bottom of the container, as sketched in Fig. 1, the gravity directs in the z direction, the bubble centroid align with the x direction, and y is another transverse direction perpendicular to the x-z plane. The three-dimensional domain is $60D$ high and has a transverse cross section of $20D \times 20D$ in order to minimum the boundary effect; note that such a computational domain is also used in our previous study about the single bubble motion [24].

The incompressible bubble flows are governed by the Navier-Stokes equations, given as

$$\rho\left(\frac{\partial \boldsymbol{u}}{\partial t} + \boldsymbol{u}\cdot\nabla\boldsymbol{u}\right) = -\nabla p + \nabla\cdot\mathbb{S} + \boldsymbol{F}_s + \boldsymbol{S}, \tag{1}$$

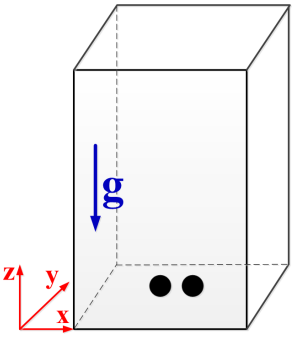

FIG. 1. Sketch of the pair of bubbles rising in viscous liquid.

$$\nabla \cdot \boldsymbol{u} = 0, \tag{2}$$

where $\mathbb{S} = \mu(\nabla \boldsymbol{u} + \nabla \boldsymbol{u}^T)$ is the viscous stress tensor, $\boldsymbol{F}_s = \sigma\kappa\delta_s \boldsymbol{n}$ stands for the surface tension force, and $\boldsymbol{S} = \rho \boldsymbol{g}$ is the gravity. In addition, ρ and μ represents the density and the dynamic viscosity of the liquid, respectively. σ is the surface tension coefficient, κ is the interface curvature, $\boldsymbol{n}$ is the normal direction of the interface, and the force confined on interface is represented by the Dirac distribution function δ_s.

A no-slip boundary condition is applied at the bottom and on the vertical lateral walls of the domain, while an outflow condition is imposed at the top. Because of the continuous VOF method employed in the present study, no extra boundary conditions are required at the bubble interface. A group of nondimensional parameters are used to describe the flow behaviors, as listed in Table I, whereas u_T is the terminal rising velocity of the bubble and the subscript 1 denotes the ambient liquid. In the list, Re describes the ratio of the inertial force to the viscous force, We is the ratio of the inertial force to the surface tension force, Mo is a dimensionless number depending on the physical properties of the liquid, Ga indicates the ratio of the gravitational force to the viscous force, and Bo indicates the ratio of the gravitational force to the surface tension force. Besides, by introducing different characteristic scales, all the variables are nondimensionalized throughout this paper: $L = L/D$, $t = tu_T/D$, $\boldsymbol{u} = \boldsymbol{u}/u_T$, and $\omega = \omega D/u_T$. In order to produce various flow environments, different silicone oils (K0–K11) are employed in the present study, and their physical properties are listed in Table II, respectively.

III. NUMERICAL TECHNIQUE, VALIDATIONS AND OVERVIEW OF THE SIMULATIONS

A. Numerical technique and validations

As aforementioned, the results discussed below are obtained by solving the three-dimensional Navier-Stokes equations in the entire fluid domain, and this is accomplished with the open-source

TABLE I. Different nondimensional parameters used to describe the bubble motion.

Name	Abbreviation	Expression
Reynolds number	Re	$\rho_1 u_T D/\mu_1$
Weber number	We	$\rho_1 u_T^2 D/\sigma$
Morton number	Mo	$g\mu_1^4/\rho_1\sigma^3$
Galilei number	Ga	$\rho_1 g^{1/2} D^{3/2}/\mu_1$
Bond number	Bo	$\rho g_1 D^2/\sigma$

TABLE II. Physical properties of different silicon oils employed in the present study.

Liquid	ρ (kg/m^3)	μ (mPas)	σ (mN/m)	Mo $= g\mu^4/(\rho\sigma^3)$
K0	761	0.49	15.9	1.8×10^{-10}
K2	873	1.75	18.7	1.6×10^{-8}
K5	918	4.59	19.7	6.2×10^{-7}
K11	935	9.35	20.1	9.9×10^{-6}

software of GERRIS flow solver [25], in which the VOF method coupled with the adaptive refinement technique (AMR) are implemented, making it a very efficient numerical tool in simulating multiphase flows. Recently, two papers used GERRIS to investigate the dynamic behaviors of the single bubble motion, by Tripathi *et al.* [27] and Cano-Lozano *et al.* [23], and both of them show very reliable results. In addition, one of our recent publications [24] also uses GERRIS code to simulate the single bubble motion, while the mechanisms of the path transition from zigzag to spiral motion are discussed. Following those studies, similar adaptive spatial resolutions are adopted herein with a grid size of $\Delta = D/64$ at the bubble interface and $\Delta = D/32$ in the wake region. The equations and the computational details implemented in GERRIS can be found in Ref. [25] and they will not be repeated here. For further verification of the usability of GERRIS in simulating the bubble motion, numerous validation cases [23,24,26,27] have been already provided, and hence they are not included here.

In particular, because the bubble interaction is a kind of special event where the thickness of the thin film between the impacting interfaces may reach the range of molecular scale [13], which is almost tens of nanometers (10^{-8} to 10^{-7} m), the attracting molecular force, namely the van der Waals force, will be dominant over other forces. This causes the bubbles to merge; otherwise, they will bounce if this critical distance is not reached before they stop moving toward each other. Therefore, much finer grids are needed in the gap to identify the thin film between the bubble interfaces. Nevertheless, the AMR techniques used in GERRIS, either based on the vorticity criterion or the curvature criterion, is not fully suitable here because they refine all the grids along the interface into the smallest size. It is unacceptable here that the computation requires huge computational resources. Therefore, we implement another AMR technique based on the topology structure to guarantee that there will be at least two grids inside the gap between the bubbles until the prescribed smallest grid is refined, as developed by Chen and Vigor [28]. Within this AMR criterion, every grid along the bubble interface will detect its neighbors in order to determine whether at least two neighbors contain either pure liquid or pure gas; if not, this grid will be refined, as shown in Fig. 2. By using this technique, only the grids inside the gap between the bubbles will be refined.

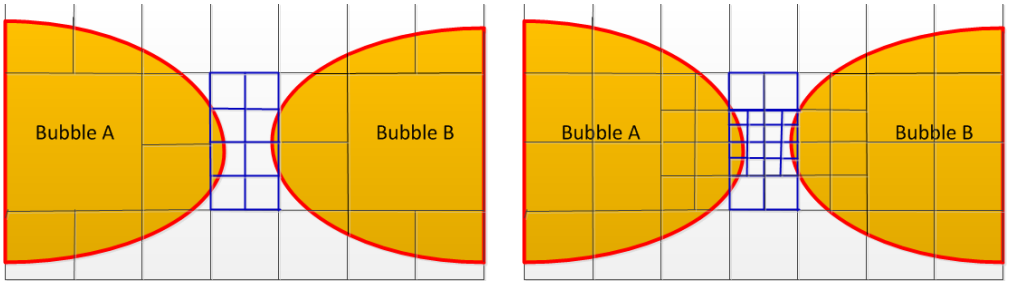

FIG. 2. The mesh distributions (a) before and (b) after performing the topology-based AMR criterion. It is observed that only the grids inside the gap between the pair of bubbles are refined.

TABLE III. Comparisons between the experimental data [13] and the numerical results obtained based on different spatial resolutions. A pair of bubbles rising in water are simulated with a size of $D = 2.8$ mm and a separated distance of $S = 1.65$.

Case	Bounce	Rising velocity (m/s)
Experiment	Yes	0.26
$\Delta = \frac{D}{800}$	No	0.265
$\Delta = \frac{D}{1600}$	Yes	0.266
$\Delta = \frac{D}{3200}$	Yes	0.267

However, it is still very difficult to conduct three-dimensional numerical simulations if the thin film is fully resolved because GERRIS restrains the level difference between the neighbor grids to not more than 1. Therefore, the number of the computational cells will increase sharply if the smallest grid size inside the gap is refined to the scale of 10^{-8} m. Meanwhile, in most cases the bubble will bounce before they reach the critical distance. Therefore, we will first determine the smallest size of the grids we need to simulate the bubble bounce by comparing our solutions with the experimental results [13].

Beside refining the grids to be $\Delta = D/64$ near the interface, much finer grids based on the topology AMR criterion are used inside the thin film, with $\Delta = \frac{D}{800}$, $\Delta = \frac{D}{1600}$, and $\Delta = \frac{D}{3200}$, respectively. The pair of bubbles of $D = 2.8$ mm are initially separated with $S = 1.65D$ in the experiments, Duineveld observed them to bounce in the water after climbing up to a certain height. The comparisons between our solutions and the experimental result are shown in Table III while the mesh distributions are presented in Fig. 3. In the table, it is found that the coarsest spatial resolution does not reproduce the bubble bounce, while the other two grids do. Meanwhile, the rising velocities agree very well with the experimental result. In addition, Fig. 3(a) shows that with the appropriate spatial discretization, the bubbles will first attract with one other and then they bounce at $H = 6$. Figure 3(b) proves that only the meshes inside the thin film are refined when they get closer, meeting

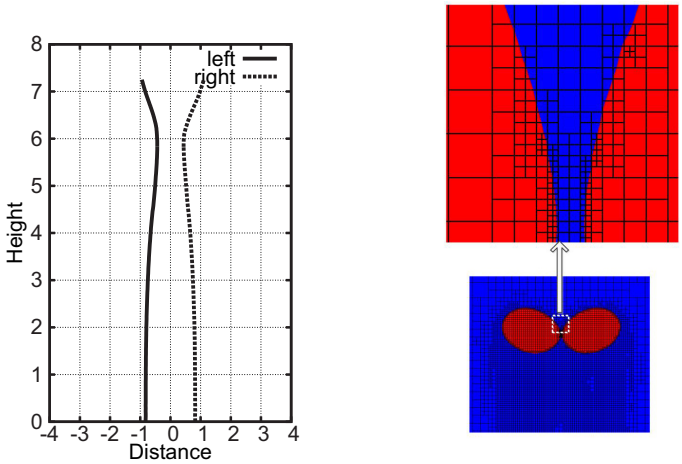

FIG. 3. (a) Calculated trajectories of the pair of bubbles under the spatial resolution of $\Delta = \frac{D}{1600}$ inside the thin film; (b) the mesh distributions close to the thin film between the two bubbles. It is observed that the bubbles will bounce off after attracting with one another at a height of $H = 6$. Moreover, only the grids inside the thin film are refined adaptively to save the computational resource.

TABLE IV. Characteristic behaviors of fifteen different bubble pairs investigated in the present study. Herein χ, Re and "isolated path" are the results for the isolated bubble, and "flow type" indicates different streamlines as shown in Fig. 5. In addition, "interaction" is the interactive behavior between the pair of bubbles, as cataloged in Fig. 7.

Case	Liquid	Mo	D (mm)	S/D	χ	Re	Isolated path	Flow type	Interaction
0	K11	9.9×10^{-6}	3.3	2.5	2.10	63	Rectilinear	*II*	Repel
1	K5	6.2×10^{-7}	1.00	2.5	1.10	17	Rectilinear	*I*	Repel
2	K5	6.2×10^{-7}	4.00	1.3	2.70	115	Unstable	$II \rightarrow IV$	Repeated bounce
3	K5	6.2×10^{-7}	4.00	1.8	2.70	115	Unstable	$II \rightarrow IV$	Repeated bounce
4	K5	6.2×10^{-7}	4.00	2.5	2.70	115	Unstable	$II \rightarrow IV$	Repeated bounce
5	K5	6.2×10^{-7}	4.00	4.0	2.70	115	Unstable	$II \rightarrow IV$	Repeated bounce
6	K2	1.6×10^{-8}	0.50	2.5	1.06	15	Rectilinear	*I*	Repel
7	K2	1.6×10^{-8}	1.40	2.5	1.46	123	Rectilinear	*I*	Attracting coalescence
8	K2	1.6×10^{-8}	1.70	2.5	1.90	180	Rectilinear	*I*	Attracting bounce
9	K2	1.6×10^{-8}	3.00	2.5	2.30	270	Unstable	$II \rightarrow IV$	Repeated bounce
10	K0	1.8×10^{-10}	0.60	2.5	1.20	133	Rectilinear	*I*	Attracting-coalescence
11	K0	1.8×10^{-10}	1.25	2.5	2.40	400	Unstable	$I \rightarrow III$	Attracting-coalescence
12	K0	1.8×10^{-10}	1.50	2.5	2.70	550	Unstable	$I \rightarrow III$	Attracting-bounce
13	K0	1.8×10^{-10}	1.50	2.0	2.70	550	Unstable	$I \rightarrow III$	Attracting-coalescence
14	K0	1.8×10^{-10}	2.00	2.5	3.20	700	Unstable	$I \rightarrow III$	Repeated-bounce

our expectations. Therefore, in the following sections, the mesh resolution of $\Delta = \frac{D}{1600}$ based on the topology AMR, together with $\Delta = \frac{D}{64}$ based on the vorticity AMR and curvature AMR, are adopted to study the interactions between the pair of bubbles. If the thickness of the film between the bubbles is thinner than $\Delta = \frac{D}{1600}$, we suppose them to coalesce numerically.

Another numerical test concerning the importance of the bulk grid refinement is further conducted on a pair of bubbles ($D = 1.7$ mm) rising in K2 with an initially separated distance of $S = 2.5D$, referring to bubble pair 8 in the following study (see Table IV). By setting the mesh size to be $\Delta = D/64$ at the interface, the pair of bubbles will bounce off at $H = 30$; however, the pair of bubbles will coalesce at the same height if we only adopt $\Delta = D/32$ at the interface. The front view of the rising trajectories of a pair of bubbles are shown in Figs. 4(a) and 4(b), while the left panel corresponds to the refined grids and the right panel is the coarse grids. Figure 4(c) displays the bounce and the coalescence between a pair of bubbles on different meshes, respectively.

B. Overview of the simulations

As indicated by Legendre and Magnaudet [9], a pair of horizontally aligned spherical bubbles will repel with one another when $\mathrm{Re} < \mathrm{Re}_{\mathrm{cr}}$ ($\mathrm{Re}_{\mathrm{cr}}$ is the critical Reynolds number which depends on their separated distance); otherwise, they will attract with one other. In their numerical investigations, the bubbles keep frozen spherical shapes so the shape deformations are not considered. However, according to more recent studies [11,12], the double-threaded wakes will not be generated behind the spherical bubble, unless it is deformed to a critical aspect ratio, which is almost $\chi = 2.2$ for an isolated bubble. As a consequence, how the double-threaded wakes affect the bubble interactions is not clear so far, and the main goal of the present study is to fill this gap.

In this paper, fifteen different pairs of bubbles have been investigated and their characteristic behaviors are listed in Table IV. In the table, D is the diameter of the equally sized bubble and S is the initially separated distance between the bubble centroid. Note that in most cases we set $S = 2.5$. χ and Re are the terminal values for the same isolated bubble motion without another bubble, and "isolated path" indicates whether the rising path of an isolated bubble is rectilinear. Notice that these

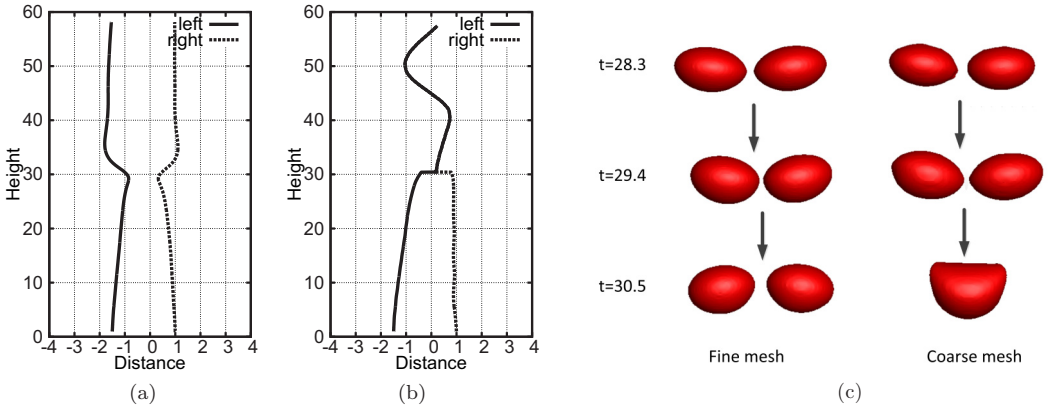

FIG. 4. Bubble pair 8 rising in K2 when the bulk spatial resolutions is different, corresponding to (a) rising paths with refined mesh ($\Delta = D/64$) at the interface; (b) rising paths with coarse mesh ($\Delta = D/32$) at the interface; and (c) interactions on different meshes. It is observed that the fine mesh guarantees the pair of bubbles will bounce off, while they coalesce on coarse mesh.

values are in good agreement with the experimental results given by Zenit and Magnaudet [29]. With respect to the "flow type" for the isolated bubble motion, it is a little complex and deserves more attention. As is widely known [30], by increasing the coming Re for a flow past the rigid sphere, the vortex structures develop in three steps: (a) $\mathrm{Re} < 24$, the flow is steady and there is no toroidal vortex rings attached at the rear of the sphere. This type of the streamlines is named flow type I in the present study. (b) $24 < \mathrm{Re} < 210$, a separation from the rear of the sphere occurs and results in the generation of axisymmetric vortex rings, and the length of the rings increases with Re but still remains stable and axisymmetric. Such streamlines around the body are flow type II. (c) $\mathrm{Re} > 210$, the flow becomes nonaxisymmetric as the ring vortex is shifted off axis and a double-threaded vortex structure is born, leading a lift force to drive the flows and becoming unstable. Such streamlines are flow type IV. In contrast, if the flow is past a spherical bubble instead of a rigid sphere, we would always obtain flow type I by increasing Re due to the slippery interface; this is already introduced in Sec. I. However, as indicated by Magnaudet and Mougin [11], increasing the aspect ratio of the bubble could lead to type II streamlines as the first bifurcation of $\chi \approx 1.7$, and subsequently, such toroidal vortex rings behind the bubble will lose the axisymmetric structure if the aspect ratio is further increased to $\chi \approx 2.2$ at the second bifurcation, and then flow type IV emerges as the flow becomes unstable. However, more recently, by using the realistic fore-and-aft shape of the bubble instead of an ellipsoid one, Cano-Lozano *et al.* [12] indicate that there is another possible way for the bubble to transit from steady to unsteady, that is from flow type I to flow type III without forming and breaking the toroidal vortex rings, while the double-threaded vortex structures are still produced. Both types of unsteady transitions, respectively, transition A (type I to type III) and transition B (type II to type IV), are described in Fig. 5, while different flow types are also labeled. Consequently, in the relevant research by Legendre and Magnaudet [9], they just consider the bubble interactions within the flows always belonging to type I. Moreover, it should be noticed that transition A always corresponds to bubble rising in low-Mo fluids, such as in water or in K0, while transition B is more likely to happen in the high-Mo fluids, such as in K5 or in K11.

In the present 15 numerical cases, the rising behaviors of the isolated bubble are positioned on the phase diagram provided by Cano-Lozano *et al.* [23], as given in Fig. 6 as a (Bo, Ga) plane where the solid line is the approximate neutral curve for the unstable transition of an isolated bubble. In addition, different flow types belonging to I–IV are labeled with different point styles, where solid square (triangle) indicates the isolated bubble to be stable while the open square (triangle) corresponds to unstable motions. Still, it should be noticed that the border between flow type III

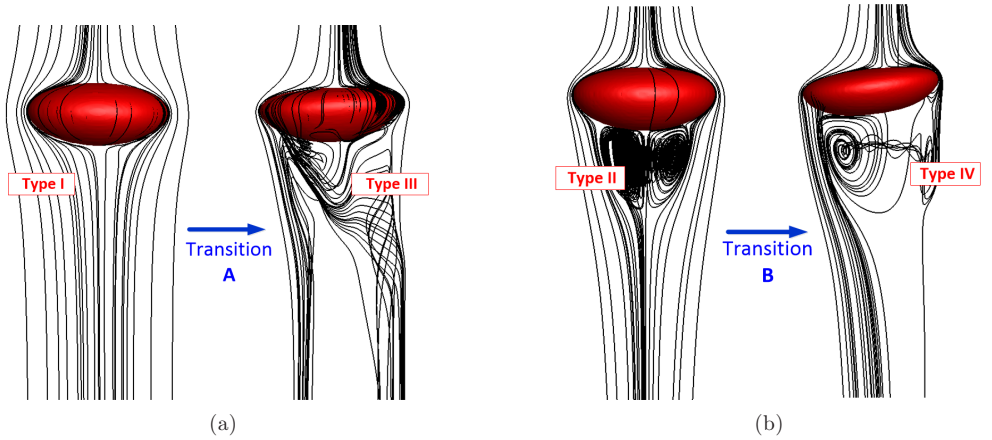

FIG. 5. Two types of unstable flow transitions around the deformable bubble. (a) Transition A from type I to type III, without forming and breaking the axisymmetric toroidal vortex rings. (b) Transition B from type II to type IV, subsequently forming and breaking the axisymmetric toroidal vortex ring.

(open square) and flow type IV (open triangle) in the unstable regime does not fully match that given by Cano-Lozano *et al.* [12], it may be ascribed to the three-dimensional simulations in the present study while they perform the two-dimensional simulations on the axisymmetric coordinate. We will show in the following study that the bubble interactions vary with differen flow types. Keep in mind that the recent paper published by Tripathi *et al.* [26] always refers to transition B within their parameter spaces under investigation. Moreover, as we will show later, in such type of flow, the bubbles always tend to repel with one another after being released, and whether they will show a repeated bounce depends on the rising behavior of the isolated bubble and the fluid properties. With respect to another type of flow transition, namely transition A, the evolution of bubble interactions is totally different from transition B, where the pair of bubbles will attract with one another after

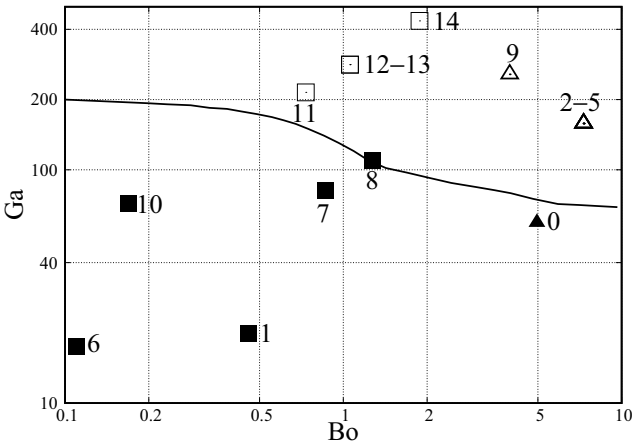

FIG. 6. Phase diagram showing the entire set of the present numerical results being positioned in the (Bo,Ga) plane, while they correspond to the isolated bubble motion. Solid line: the approximate neutral curve for the unstable transition of an isolated bubble [23]. ■, Type I flow; ▲, type II flow; □, type III flow; and △, type IV flow.

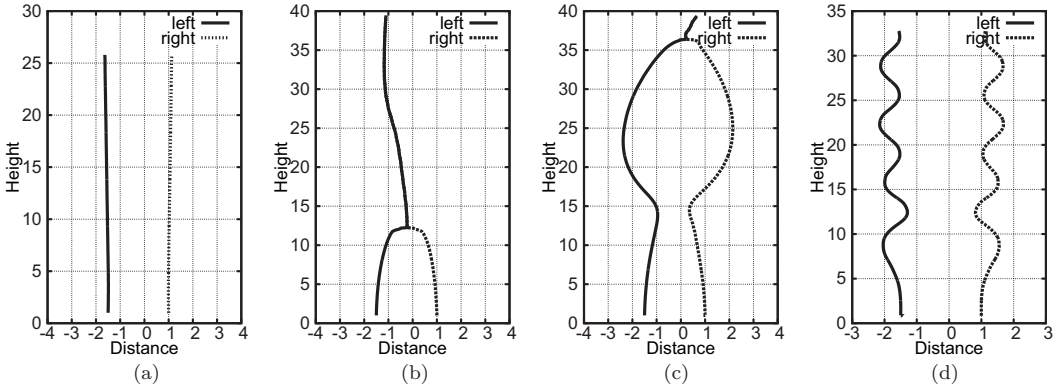

FIG. 7. Four typical interactions between a pair of bubbles, corresponding to (a) bubble pair 1, repelling; (b) bubble pair 11, attracting coalescence; (c) bubble pair 12, attracting bounce; and (d) bubble pair 4, repeated bounce. The horizontal axis is the position of the bubble centroid and the vertical axis is the rising height, and both axes are nondimensionalized by the bubble diameter.

being released. During the approach, they will probably show coalescence or bounce depending on the fluid properties, the separated distance between a pair of bubbles, and the bubble size.

With respect to "interaction" in the last column of Table IV, typical interactive behaviors are presented in Fig. 7, whereas repelling, attracting coalescence, attracting bounce, and repeated bounce are obtained in the present numerical study. Table IV clearly indicates that the interactive behaviors between the pair of bubbles are greatly dependent on the flow conditions and bubble pair characteristics. In addition, similar experimental studies were conducted by Duineveld [13] and Sanada *et al.* [14], who found different interactions between the pair of bubbles, i.e., coalescence or bounce after approaching, were determined by the collision velocity or rising velocity. However, the present study aims to investigate the underlying mechanisms responsible for different interactions, particularly of the evolutions of the wake vortices during the bubble interactions.

IV. OBSERVED PATHS AND WAKES OF A PAIR OF BUBBLES RISING WITHIN FLOW TYPE I

In this section, we comment on different bubble interactions within flow type I, focusing on the relation between the interactive paths and the wake developments. We will also show that the interactive behaviors actually depend on several factors, such as low- and high-Re flow regimes, stable and unstable isolated bubble motion, separated distance, and bubble size. Emphasis is put on the discussion of the underlying mechanisms in order to identify the causes or the nature of different interactions, and we comment on the importance of the wake developments during the bubble collision.

A. Isolated bubble rising in rectilinear path: Low-Re regime

As indicated by Legendre and Magnaudet [9], two spherical bubbles belonging to flow type I will repel with one another in the low-Re regime. Two cases are investigated in the present study, respectively, of bubble pair 1 and bubble pair 6, for which the terminal (Re, χ) correspond to (17, 1.1) and (15,1.06), respectively. Herein, bubble pair 1 is taken, for instance, and the rising trajectories of the bubble centroid are presented in Fig. 8(a), where the two bubbles repel one another within the pair. As interpreted in that paper, the vorticity diffusion near the bubble surface is blocked in presence of another bubble in such a situation, and hence the distribution of the vorticity becomes strongly asymmetric and causes the repulsive force generated between the pair of bubbles. This is

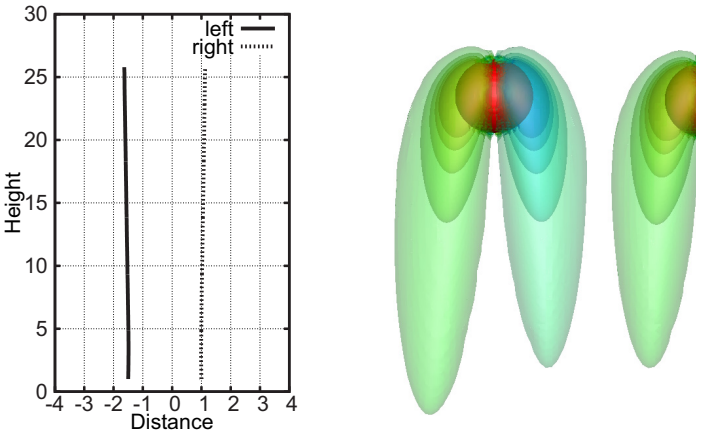

FIG. 8. Repulsive interactions between bubble pair 1, corresponding to flow type I in the low-Re regime (Re < 30). (a) Bubble trajectories. (b) The isocontours of ω_y around the bubbles, corresponding to $-100 < \omega_y < 100$. The result reveals that the vorticity diffusion is blocked in presence of another bubble, and hence the repulsive force is generated.

more illustrative by plotting the distribution of ω_y around the bubble, as shown in Fig. 8(b), where the diffusion of the inner vortices are blocked by another bubble.

B. Isolated bubble rising in rectilinear path: Moderate-Re regime

In contrast to the low-Re regime, if the terminal Re of the rising pair of bubbles becomes higher while the path of the isolated bubble still keeps rectilinear, the pair of bubbles will always attract with one another after being released due to the Venturi effect where the pressure is lower inside the gap between the pair of bubbles. Bubble pair 10 and bubble pair 7 are selected for investigation because their terminal Re are close to $\approx O(120)$ while their aspect ratios are varied as $\chi_{10} = 1.2$ and $\chi_7 = 1.46$ as shown in Table IV. Their trajectories are presented in Fig. 9 and attraction-coalescence interactions are observed in both displays, while the coalescence time is delayed in bubble pair 7, indicating that the attractive force between the two bubbles within the pair becomes weaker with larger χ. Besides, at the moment when coalescence happens, the flow streamlines and the streamwise vortices with respect to $\omega_z = \pm 2$ in vicinity of the bubbles are also presented in Fig. 9, and it is obvious that neither the attached toroidal vortex rings nor the streamwise wakes are generated behind the pair of bubbles at the "kissing" moment.

For the coalescence process, bubble pair 7 is discussed herein and the evolvement of the rise velocities is presented in Fig. 10(a) before and after the coalescence. The rising velocity is observed to drop at $t = 240$ first, from $u_z = 1$ to nearly $u_z = 0.6$, and subsequently a periodic oscillation is followed after the coalescence. As indicated by Duineveld [13], the oscillation results from the difference in surface energy between the coalesced larger bubble and the two original smaller bubbles, and then the oscillatory frequency during the coalescence stage is found to follow the second mode [13,14], that is, $f_2 = \frac{1}{2\pi}\sqrt{\frac{96\sigma}{\rho D^3}}$. Accordingly, the dimensional frequency of the second oscillation mode should be $f_2 = 137.85$ Hz for bubble pair 7, and this seems to be in excellent agreement with our numerical results of $f = 140.8$ Hz. However, it should be noted that the coalescence in numerical simulation is not a fully physical process but we can still obtain a very reasonable estimate of the oscillation frequency by considering only the contribution from surface

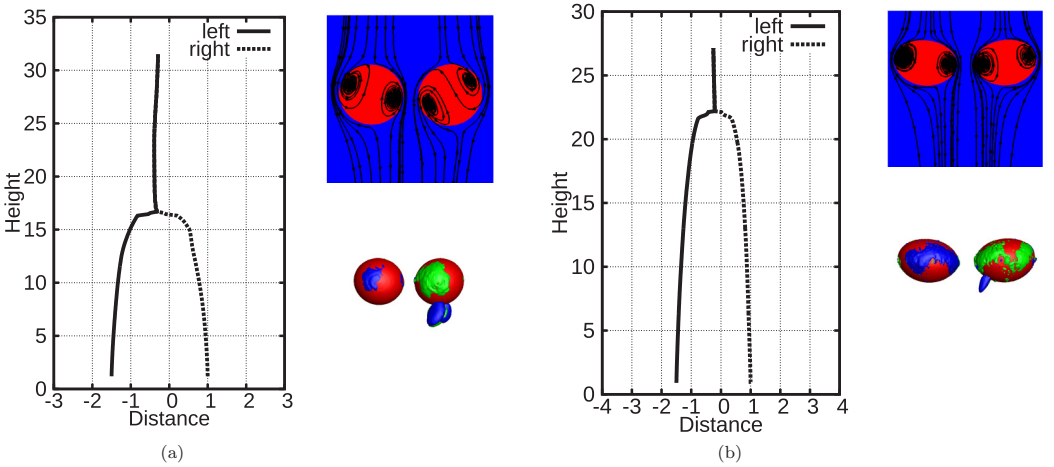

FIG. 9. Interactions between bubble pair 10 and bubble pair 7 where the isolated bubble rises rectilinearly in both cases. (a) Bubble pair 10 with terminal state of Re = 133 and $\chi = 1.2$. Bubble pair 7 with terminal state of Re = 123 and $\chi = 1.4$. The right panel of each subfigure is the streamlines around the pair of bubbles and the streamwise vorticity isocontours of $\omega_z = \pm 2$ before the bubbles kiss each other. It is found that no torodial vortex rings or streamwise wakes are generated behind the pair of bubbles at the "kissing" moment.

tension. Moreover, the time histories of the bubble shapes are presented in Fig. 10(b) during the coalescence, and the whole attraction-coalescence-oscillation process is clearer.

However, it does not necessarily mean that an isolated bubble rising in a rectilinear path will always coalesce with another bubble when they rise side by side; they also probably bounce off after "kissing," and this situation is discussed by taking bubble pair 8, for instance. Keep in mind that for this case, the aspect ratio of the bubble pair is $\chi_8 = 1.9$, which is still below but very close to the critical aspect ratio to trigger the path instability for an isolated bubble rising in K2, which is $\chi_{K2} \approx 2.05$ [29]. Front views of the rising trajectory of bubble pair 8 and the isolated bubble are plotted in Figs. 11(a) and 11(b), respectively. For the pair of bubbles, it is found that they bounce off at a height of $H = 30$ after approaching, and following the collision, the bubbles start to rise rectilinearly so no more path instability is observed. Accordingly, for the isolated bubble case, it always maintains the rectilinear motion, corresponding to what is observed in experiments [29].

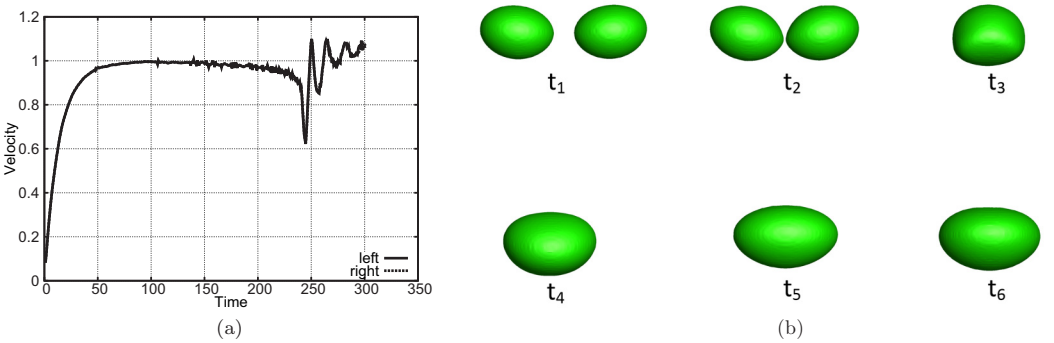

FIG. 10. Oscillations during the coalescence between bubble pair 7. (a) The rise velocities. (b) The bubble shape evolutions with a time interval of $\Delta t^* = 13$. Significant oscillations are observed during the coalescence process.

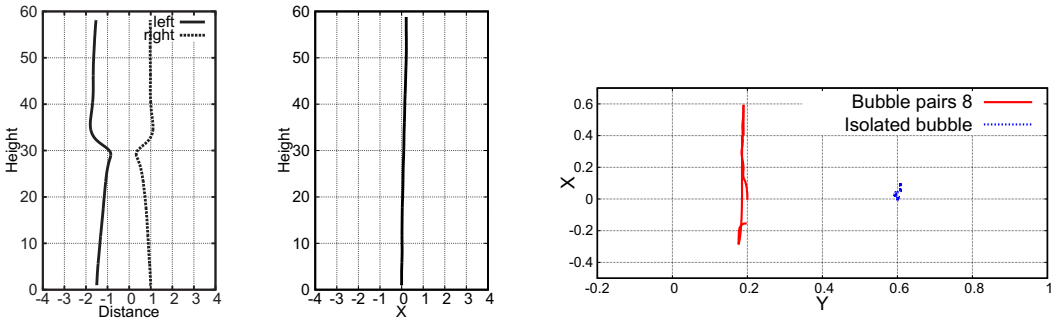

FIG. 11. Rising trajectories of bubble pair 8 and the corresponding isolated bubble. (a) Front views of bubble pair 8; (b) front views of the isolated bubble; and (c) top views of the (left) bubble [note that coordinate transformations are applied to make the (left) bubble rise from $x = 0$]. It is observed that although the isolated bubble rises rectilinearly, the pair of bubbles still show an attracting-bounce interaction behavior.

This difference is more visible from the top view of the trajectories, as depicted in Fig. 11(c), whereas the left curve is the left bubble within the bubble pair while the right curve corresponds to the isolated bubble. It should be noted that a coordinate transformation is applied to put the two paths in a single picture so that both bubbles could rise from $x = 0$. Obviously, the isolated bubble shows a nearly rectilinear path so that little transverse motion is observed. However, for the left bubble in the bubble pair, it first moves toward the $x+$ direction and then turns to a reversed motion along the $x-$ direction, which forms one period of zigzag motion. Emphasis is put on the discussion of the underlying mechanisms that cause the bubble bouncing. In this case, as is widely known, the generation of the double-threaded streamwise vortices are responsible for the path instability of an isolated bubble so that a critical aspect ratio of the bubble shape should be reached to induce the vortex shedding. Therefore, the bounce behaviors in bubble pair 8 indicate that the threshold for the generation of the double-threaded vortices is reduced in the presence of another bubble. Correspondingly, the evolution of the wake structures during and after the collision in bubble pair 8 is presented in Fig. 12(a). In the figure, it is observed that the double-threaded vortex structures are generated when the two bubble get close, and during the collision, the wake-induced lift forces repel the bubbles away while the vortices are detached from the bubble interface. After the two bubbles are separated to some distance, no additional vorticities are produced at the bubble interface so that no double-threaded vortices are shed from the interface any more, and hence the bubbles do not show any path instability. This is understandable because an isolated bubble always rises rectilinearly and that not enough vorticities will accumulate at the bubble interface to generate the double-threaded-vortex structures. More importantly, the time histories of total amounts of ω_z accumulated on the interface of the (left) bubble, i.e., $\Omega = \int_S \|\omega_z\|$ where dS is the bubble surface and $\| \ \|$ is the norm of ω_z, are also presented in Fig. 12(b), whereas the open circle indicates the time instants when bounce happens in bubble pair 8. For the isolated bubble, the curve is nearly flat after the starting period of the bubble rising, and Ω always stays at a relative low level of $\Omega = 5$. However, for bubble pair 8, Ω is increased sharply as the bubbles get closer during the time period of $20 < t < 29$, and finally the critical value of $\Omega \approx 10$ is attained around $t = 29$ so that the double-threaded vortices are born to separate the pair of bubbles. After the bubbles are fully separated, i.e., $t > 35$ as indicated from Fig. 12(a), the vortex accumulation on bubble pair 8 drops to the same level of that in an isolated bubble case, staying at $\Omega = 5$. Therefore, it clearly indicates that the interactions between the pair of bubbles greatly depend on the amounts of ω_z accumulated on the bubble interface, and we will show in Sec. VI B that the drag force is also increased correspondingly due to the vorticity accumulations.

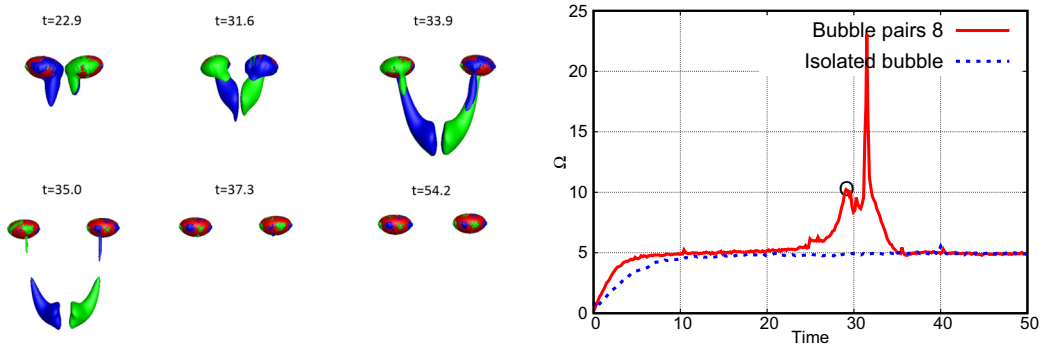

(a)evolution of vortex structures (b)history of Ω

FIG. 12. (a) Evolution process of the double-threaded wakes during the collision of bubble pair 8, while the isocontours correspond to $\omega_z = \pm 1$. (b) Amount of ω_z accumulated at the (left) bubble interface. For an isolated bubble, Ω almost stays at a relative stable and low value of $\Omega = 5$; however, for bubble pair 8, Ω increases sharply to trigger the vortex shedding as the bubbles get close, indicating that only if the streamwise vorticity accumulated on the bubble surface is more than a critical value, then the double-threaded wakes would be generated to cause bubble collision.

C. Isolated bubble rising in unstable path

When the isolated bubble shows unstable motion, i.e., zigzag or spiral, bubble pair 12 is investigated and the rising trajectories of the left isolated bubble are plot in Fig. 13. From the top view, it is observed that the isolated bubble shows oscillations in the transverse direction, which indicates its motion to be already unstable. From the front view, the bubble pair first attracts one another and a bounce follows; after that, the bubbles approach again and finally coalesce at $H = 36$. Because we think the bubble wakes play a key role in determining whether the bubbles will bounce or coalesce after approaching one another, the developments of the streamwise wake vortices are expected to be different at the "bouncing moment" and the "coalescence moment." Accordingly, the wake structures corresponding to $\omega_z = \pm 2$ are plotted in Fig. 14, where this evolution process can be divided into two stages, with respect to attracting bounce and attracting coalescence, respectively.

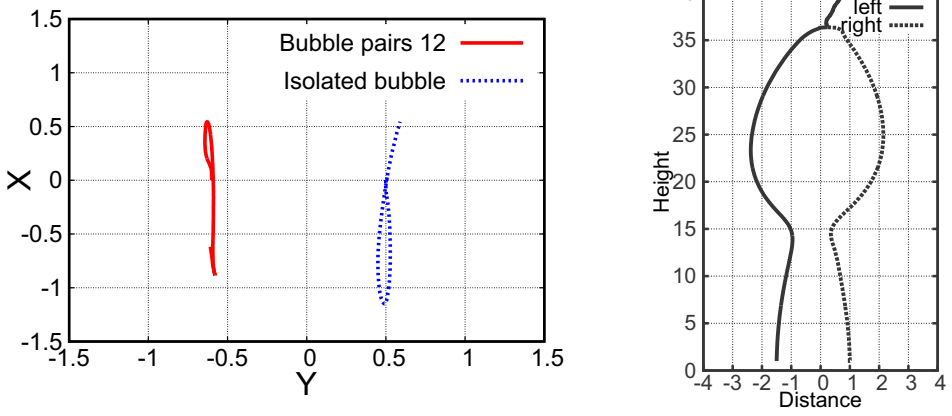

FIG. 13. Rising trajectories of bubble pair 12 and the corresponding isolated bubble. Detailed description is provided in the caption of Fig. 11. It is observed that while the isolated bubble rises in an unstable path, the bubble pair shows an attracting-bounce interaction followed by another attracting-coalescence interaction.

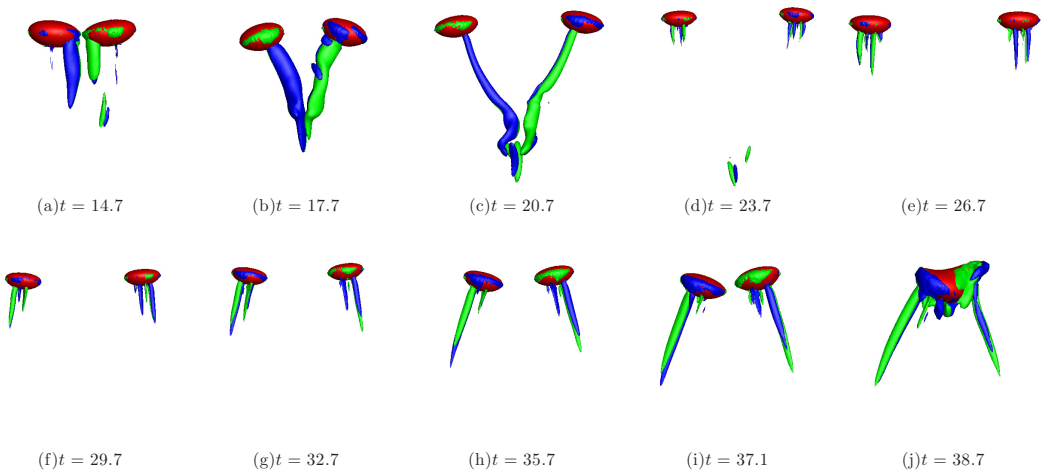

FIG. 14. Evolution process of the double-threaded wakes during the attracting-bounce period and the following attracting-coalescence period for bubble pair 12. [(a)–(e)] The two bubbles bounce off and move outward to the furthest position; [(f)–(j)] the two bubbles attract one another until coalescence. In all figures, isocontours correspond to $\omega_z = \pm 2$.

In the first stage, the two bubbles bounce off at $t = 14.7$ and then moving outward until reaching the furthest positions at $t = 26.7$. During the bubble collision, the double-threaded wakes are generated at the inner side of the bubbles, causing the two bubbles to bounce off. Meanwhile, the interactions between the wakes are very similar to the experimental study conducted by Sanada *et al.* [8]. In their experiments, the authors propose that the bubble wake dominates the process of the bubble bouncing, but they do not give clear interpretations. After the bubbles move outward, i.e., at $t = 23.7$, the double-threaded wakes in the inner sides disappeare gradually due to the viscous dissipating. At $t = 26.7$, the bubbles reach the furthest positions and other vortex pairs to drive the bubbles inward are generated at the outsides of the two bubbles. However, the vortex strengths look much weaker in comparison with those during the first touch. In the second stage, from $t = 29.7$ to 41.7, the two bubbles attract one another again and finally coalesce after "kissing." During this period, nevertheless, no new wakes are generated in the inner sides, and therefore the pair of bubbles do not bounce off again because the vortex interactions at the inner sides are rather weak.

However, for an unstable isolated bubble, the result does not necessary indicate that the corresponding pair of bubbles will always bounce off each other during the collision, because some other factors also take effect, such as the initially separated distance and the bubble size, while other flow conditions remain unchanged, and both factors are investigated in experiments by Duineveld [13] and Sanada *et al.* [8], who ascribe different interactions to varied bouncing velocities if the separated distances or bubble sizes are changed. However, in the present study, the main focus is still put on the developments of bubble wakes within different flow conditions. First, we will study the influence of the initially separated distance S that the contrast numerical test is shown in bubble pair 13 by shortening the separated distance from $S = 2.5$ to $S = 2.0$, and the rising trajectories of bubble pair 12 and bubble pair 13 are presented in Figs. 15(a) and 15(b), respectively. It is observed that in contrast to the bouncing interaction within bubble pair 12, the bubble pair 13 coalesces directly at $H = 7$ without bounce. Since we believe the wake developments dominate the bubble collisions, as a consequence, it is expected that in the case of $S = 2.5$, there is enough time for ω_z to accumulate at the bubble interface, and hence the double-threaded vortex structures are generated to repel the pair of bubbles. However, in the case of $S = 2.0$, in which the distance between the pair of bubbles is not large enough, there would not be enough ω_z accumulated at the bubble interface due to time limit before "kissing" and therefore no double-threaded vortex

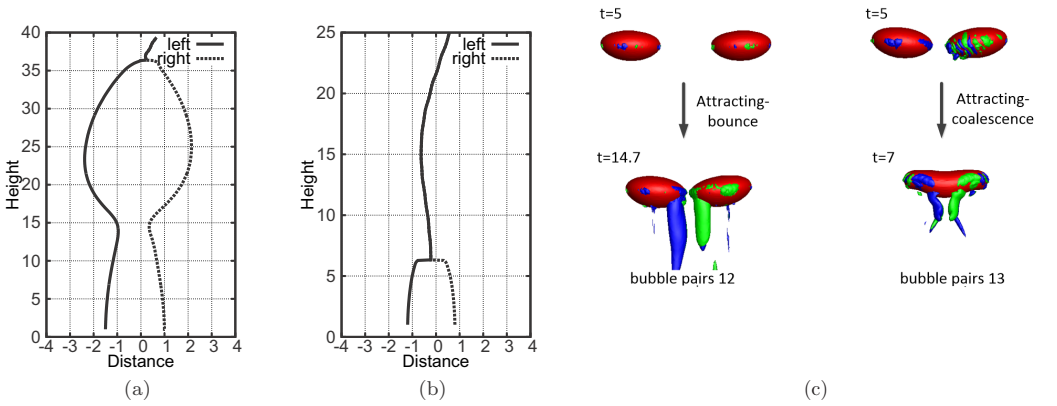

FIG. 15. Interactions between the pair of bubbles rising in K2 when the initial separated distance is changed. Bubble pair 12 with $S = 2.5$; bubble pair 13 with $S = 2.0$; (c) different wake developments during bubble interactions. It is observed that with larger distance, the pair of bubbles are more likely to bounce off instead of coalescence, and this is closely related to the wake developments behind the pair of bubbles.

structures would be generated. Such conjectures are validated in Fig. 15(c), whereas the left panel describes the isocontours $\omega_z = \pm 2$ for bubble pair 12 at different time instants before the bubbles bounce off, and the right panel is for bubble pair 13 at the moment of coalescence. In the figure, it is obvious that at $t = 5$, both bubble pairs do not produce double-threaded wakes, and therefore bubble pair 13 coalesces directly. However, for bubble pair 12, whose bubbles have extra time to move closer to each other, stronger vortex pairs are generated at $t = 14.7$, and hence they bounce off. Our explanations could also interpret some of the experimental results observed in water belonging to flow type I, as presented by Duineveld [13], who found the pair of bubbles rising in water were easier to bounce off if they were separated by a larger distance. However, they thought it was the collision velocity, which was greater by widening the initially separated distance, that caused the bubbles to bounce. As a consequence, we would like to present the temporal variations of the transverse velocity of the left bubble within the two bubble pairs in order to investigate the influence of the collision velocity on the bubble interactions, as shown in Fig. 16. First, bubble pair 12 bounces off at point B while bubble pair 13 coalesces at point A; however, the collision velocity is observed to be much larger in bubble pair 13 than in pair 12, indicating that greater collision velocity does not necessary mean bouncing between the bubbles, and this observation is in contrast that of with Duineveld [13]. Second, for bubble pair 12, the bubbles bounce off at point B while they coalesce at point C; however, we still find the collision velocity to be larger at the collision moment. Therefore, it is more likely the vortex interactions rather than the collision velocity to determine whether the pair of bubbles will bounce or coalesce when they "kiss" with one another.

The second influential factor, namely the bubble size D, is also investigated in the present study in which bubble pair 11 ($D = 1.25$ mm), bubble pair 12 ($D = 1.5$ mm), and bubble pair 14 ($D = 2.00$ mm) rising in K0 are simulated. Their rising trajectories are presented in Fig. 17 and the attracting coalescence, attracting bounce, and repeated bounce are observed in succession, indicating that the repulsive effect between the pair of bubbles is more significant as D is increased. Likewise, different interactive behaviors must be ascribed to different wake structures depending on the bubble deformations in which larger bubbles lead to greater shape deformations, and correspondingly, the streamwise vortex structures behind larger bubble pairs are stronger and hence greater repulsive forces are generated accordingly. The vortex structures with different bubble sizes are not presented here because similar contour maps corresponding to the coalescence and bounce interactions have been plotted previously. Instead, the repeated bounce of bubble pair 14 is discussed

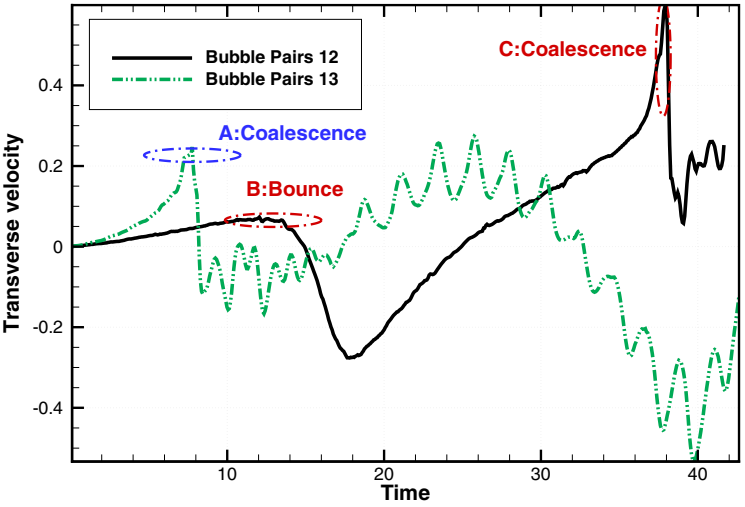

FIG. 16. Temporal variations of the transverse velocity of the left bubble in bubble pair 12 and bubble pair 13. Point A: coalescence of bubble pair 13. Point B: bounce of bubble pair 12. Point C: coalescence of bubble pair 12. It is found greater collision velocity does not necessarily indicate bouncing interactions between the pair of bubbles.

here in that the evolutions of the bubble wakes corresponding to $\omega_z = \pm 2$ are plotted in Fig. 18, whereas four typical time points are selected during one repeated-bounce period, passing the average and extreme positions. It is observed that the streamwise vortices are to be shed alternatively at both sides of the bubble, and this is very similar to what is observed for a zigzagging isolated bubble [23,24]. However in this case, the wake instability seems to be significant in that the long vortex threads tend to twist with one another and the shear instability is observed at the tail of these threads, which should be attributed to the relatively high-Re flow. Note that another group of

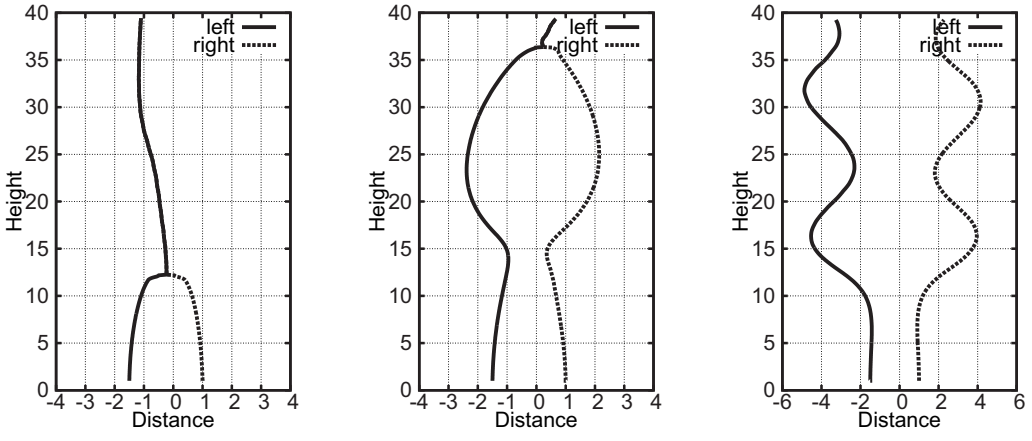

FIG. 17. Trajectories of the pair of bubbles rising in K0 when the bubble sizes are varied. (a) Bubble pair 11 with $D = 1.25$ mm, (b) bubble pair 12 with $D = 1.5$ mm, and (c) bubble pair 14 with $D = 2$ mm. It is observed that by increasing the bubble size, attracting coalescence, attracting bounce, and repeated bounce appear in succession between a pair of bubbles.

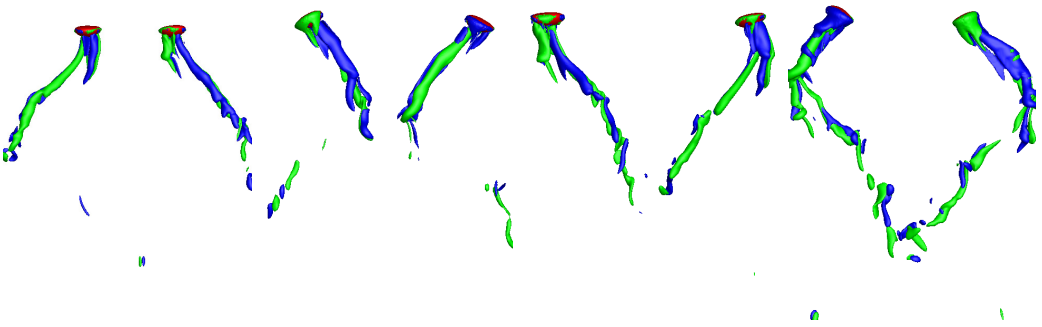

FIG. 18. Wake structures behind the bubble pair 14 at different time periods during a repeated-bounce period, and the isocontours correspond to $\omega_z = \pm 2$. It is observed that periodic vortex shedding happens while the wake is unstable at the tail due to viscous shear.

numerical tests about the influence of bubble sizes on the bubble interactions are also carried out in K2 as bubble pair 7, bubble pair 8, and bubble pair 9; nevertheless, the results are very similar with this group conducted in K0, and hence they will not be discussed here any more.

To summarize, some of the available experimental observations about the pair of bubbles rising in water can be interpreted based on the present numerical results. According to Duineveld [13], the pair of bubbles with size smaller than $D = 0.7$ mm would never bounce off but always coalesce in the water, regardless of the separated distance. It was thought that the collision velocity was too small to induce the bounce behavior between the pair of bubbles. More than that, our numerical results show underlying mechanisms: Because smaller bubble pair almost remain spherical during rising, double-threaded wakes cannot be generated behind them to repel the bubbles. The same principle can be also applied to interpret why a long separation distance S is required to induce bouncing between a pair of bubbles because small separation distance is not able to generate the double-threaded vortex structures during the collision.

V. OBSERVED PATHS AND WAKES OF A PAIR OF BUBBLES WITHIN FLOW TYPE II

In the available experimental studies, most of the emphasis is put on the pair of bubbles rising in water which belongs to flow type I (or transition A); however, for another situation as stated previously, flow type II (or transition B) with toroidal vortex rings attached behind the bubble also exists in some high-Mo fluids. We will show in this section that the existence of such vortex structures makes the interactions between the pair of bubbles totally different from those rising in flow type I.

A. Isolated bubble rising in rectilinear path

As already indicated in Sec. IV, for an isolated bubble rising in a rectilinear path, the corresponding bubble pair rising within flow type I will either repel or attract one another depending on the rising Reynolds number. However, for flow type II, things are different that the pair of bubbles are always found to repel with one another, and one test case of bubble pair 0 is investigated that the rising trajectories of the pair of bubbles are presented in Fig. 19(a), whereas the repulsive interaction is observed all the time. It should be noted that the rising path of the isolated bubble is rectilinear; therefore, it is the presence of another bubble to trigger such transverse "repulsive" motion. Again, we ascribe this to the wake effect. The flow streamlines around the left bubble are plotted in Fig. 19(b), whereas the inner toroidal eddies behind the bubbles are squeezed in the presence of another bubble, and then the axisymmetry vortex structure is broken so that the flow

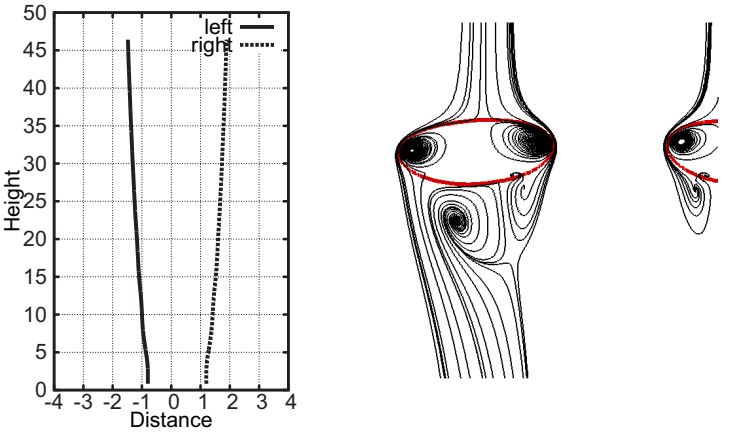

FIG. 19. Interaction behaviors between bubble pair 0, corresponding to an isolated bubble rising rectilinearly within flow type II. (a) The rising trajectories; (b) the flow streamlines around the pair of bubbles. It is observed that the toroidal vortex rings become asymmetric in the presence of another bubble.

transition B is triggered to induce a transverse repulsive force. Therefore, the mechanisms for the generation of this repulsive force, correspondingly, are thought to be different from that in bubble pair 1 in the low-Re regime of flow type I, as introduced in Sec. IV A. Furthermore, we would like to investigate how the toroidal vortex rings become asymmetrical in the presence of another bubble. For an isolated bubble of bubble pair 0, the coming flow is uniform, and hence the toroidal vortex rings behind the bubble are also axisymmetric, as shown in Fig. 20(a). Nevertheless, with respect to the motion of the pair of bubbles, as shown in Fig. 20(b), the coming flow past through the gap is faster, and consequently, the shear rate inside the gap is more significant, which causes the inner vortex rings to be squeezed. This observation is very similar to the situation when a sphere rises parallel to a vertical wall [31]: The vortex rings are also formed at the rear of the sphere, and the

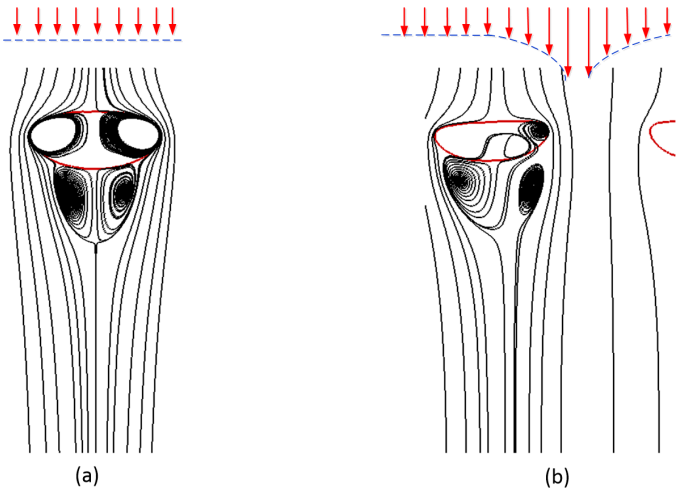

FIG. 20. Different curvatures of the fluid velocity profile on the flow around the bubble. (a) Isolated bubble; (b) a pair of bubbles.

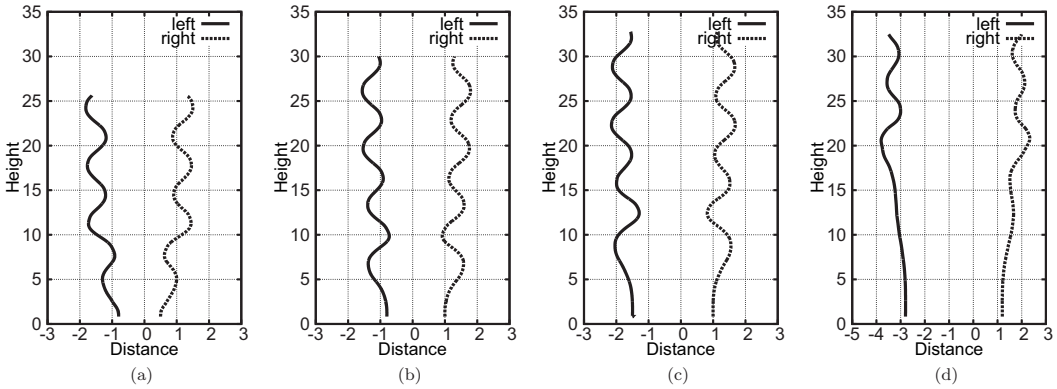

FIG. 21. Rising trajectories of a pair of bubbles in K5 with varied initially separated distance. Note that these cases belong to flow type II. (a) Bubble pair 2 with $S = 1.3$, (b) bubble pair 3 with $S = 1.8$, (c) bubble pair 4 with $S = 2.5$, and (d) bubble pair 5 with $S = 4.0$. It is observed that with smaller S, the repeated bounce happens earlier while the bounce frequency and the bounce amplitude are almost the same.

results indicate the strengthened shear rate inside the gap between the sphere and the wall would destroy the axisymmetry of the standing eddy and thereby the repulsive lateral force is induced.

After being repelled, bubble pair 0 are not observed to attract one another again, indicating that the rising paths of the two bubbles are still stable without oscillations. However, Tripathi *et al.* [26] observe that even if the isolated bubble travels in a rectilinear path within flow type II, there is a possibility for the pair of bubbles to exhibit a repeated-bounce behavior, and this is more evident with a smaller separated distance. However, in their numerical simulations, such phenomena only happen when the pair of bubbles rise in a fluid of Mo $\sim O(1.0 \times 10^{-4})$, which is much higher than what we investigate herein, Mo(K11)$\sim O(1.0 \times 10^{-5})$. Consequently, we think that after repelling, whether the pair of bubbles will always repel with one another or are followed by a subsequent repeated-bounce interaction greatly depends on the rising behaviors of the isolated bubble and the fluid properties.

B. Isolated bubble rising in unstable path

For an unstable isolated bubble rising within flow type I, it is revealed in Sec. IV C that the pair of bubbles will show either an attracting-coalescence behavior or an attracting-bounce behavior depending on the flow conditions. However, for such unstable isolated bubble rising case within flow type II, the bubbles will always show a repeated-bounce interaction where the differences between them are the following: The transition moment for the path instability is brought forward earlier in the presence of another bubble and the smaller the initial separated distance, the earlier the repeated bounce happens. By changing the separated distances between the pair of bubbles while maintaining other parameters unchanged, namely bubble pair 2–5, their rising trajectories can be plotted as in Fig. 21. In different cases, the pair of bubbles are separated with distances of $S = 1.3$, $S = 1.8$, $S = 2.5$, and $S = 4.0$ respectively, and similar repeated bounces are observed between the pair of bubbles where the aptitude and the frequency of the path oscillations are almost the same. If the separated distance is as small as $S = 1.3$, the repeated bounce happens much earlier as long as they start to rise. However, if the separated distance is increased to $S = 4.0$, the bubble motion is almost independent of another one at first, taking a long time to enter the repeated-bounce motion. It is obvious that the initially separated distance greatly influences the interactive behaviors between the pair of bubbles, because a smaller S favors breakup of the axisymmetric toroidal vortex rings by generating stronger shear inside the gap, as already indicated in Fig. 20. To further identify that the repeated-bounce behavior is actually a manifestation of the zigzag motion, the temporal variations of the transverse velocity of the left bubble in different bubble pairs are plotted in Fig. 22(a). It

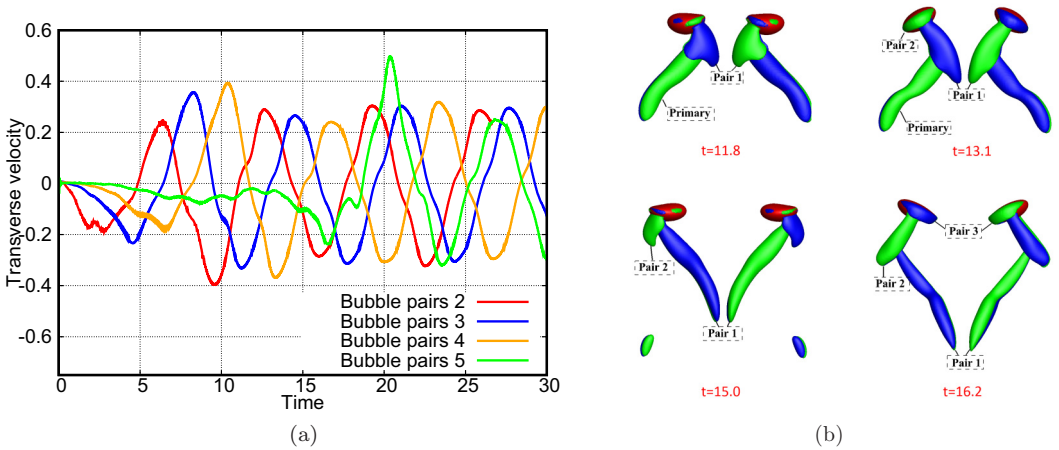

FIG. 22. (a) Temporal variation of the transverse velocity of the left bubble in bubble pair 2–5. It is observed that with a smaller separated distance, the repeated bounce happens earlier. However, once they enter the repeated-bounce motion, the frequency and amplitude of the velocity oscillations are the same, indicating that the repeated-bounce behavior is actually a particular type of the zigzag motion. (b) Isocontours $\omega_z = \pm 2$ at four successive time points when the bubbles pass the average and furthermost (nearest) positions corresponding to bubble pair 4. It is observed that the double-threaded wakes are generated behind the pair of bubbles, while their signs are changed periodically during the repeated-bounce process.

is found that once the pair of bubbles enter the repeated-bounce motion, all four cases settle into the same frequency and amplitude of the speed oscillations, and hence they are actually the same zigzag motions except that smaller separated distance is apt to trigger the zigzag motion earlier. In addition, note that no collisions are observed between the pair of bubbles before the emergence of the repeated-bounce motion, which is more like a contactless way. Furthermore, the isocontours $\omega_z = \pm 2$ of bubble pair 4 are also presented at four successive time points when the bubbles pass the average and furthermost (nearest) positions, as shown in Fig. 22(b). From the figure, it is found the evolutions of the double-threaded wakes are exactly the same as what we observe during the zigzag motion of an isolated bubble [24]. Similarly, the evolution process can be summarized as follows: (a) When both bubbles reach the nearest (resp., furthest) position, the shedding vorticies at the inner side (resp., outer side) will generate a transverse vortical force directing outward (resp., inward), and then the bubbles move outward (resp., inward). During this period, new vorticities begin to gather at the lateral surface of the bubbles. (b) When the bubbles pass the average position, the amount of the gathered vorticities on bubble surface reaches the critical value and a new round of vortex shedding process begins. During this stage, the new double-threaded wakes are generated with opposite signs.

Top views of the rising trajectories for bubble pair 2–5 are shown in Fig. 23, and the rising path of an isolated bubble is also investigated for comparison. In the figure, top views of the rising trajectory of the left bubble in a pair of bubbles separated by $S = 1.3$, $S = 1.8$, $S = 2.5$, $S = 4.0$, and $S =$ infinity (isolated bubble) are presented from left to right. It is interesting to notice that the isolated bubble is rising in a spiral motion developed from a zigzag stage, which is identical to the phase diagram given by Cano-Lozano *et al.* [23] according to the parameter space of {Ga,Bo} = {158.4, 7.3}. However, by placing another bubble aside, i.e., $S = 4.0$ away from the isolated bubble, the spiral motion is suppressed in the y direction that a zigzag-like motion is generated gradually. Furthermore, if the separated distance is further decreased, typically from $S = 4.0$ to $S = 1.3$, the zigzag motion is more perfect as the oscillation in the y direction has almost disappeared. As a consequence, it seems that for an unstable isolated bubble rising in flow type II, whether rising in a zigzag motion or in a spiral motion, a pair of bubbles are restricted to only oscillate in the $x-$

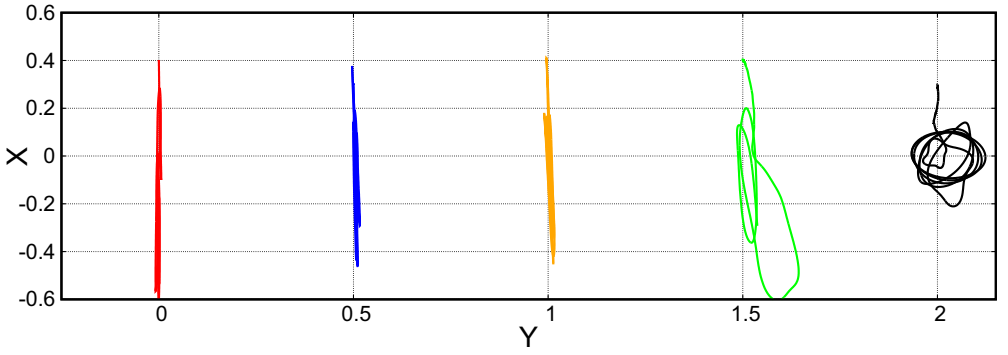

FIG. 23. Top views of the trajectory of the left bubble in different bubble pairs, from left to right: bubble pair 2–5 and the isolated bubble. It is observed that while an isolated bubble shows a zigzag-spiral transitional motion, in the presence of another bubble rising side by side, a more perfect zigzag motion is generated by shortening the separated distance between the pair of bubbles.

direction that a zigzag motion is always formed. That is because in the presence of another bubble rising side by side, the axisymmetric toroidal vortex rings will always first break at the inner side between the pair of bubbles, and hence, the lift force also is directed along the bubble centroid and it will not move to the azimuthal direction to trigger a spiral motion.

As previously indicated [24], the amounts of the streamwise vorticities (ω_z) accumulated at the bubble surface are found to be of great importance in triggering the path instability for an isolated bubble motion; that is, when $\Omega = \int_S \|\omega_z\| dS$ reaches a critical value, the vortices will shed from the bubble interface and hence the path instability happens. With respect to the present situations, the time histories of Ω calculated on the left bubble are plotted in Fig. 24, whereas the isolated bubble case is also computed as comparison. Note that since the isolated bubble takes a long time to trigger the vortex shedding, and only the development of Ω after $t > 25$ is plotted and the actual time is $t' = t - 25$ to make the figure more readable. The result indicates the smaller the separated distance, the quicker the accumulation of ω_z at the bubble interface, and hence an earlier vortex

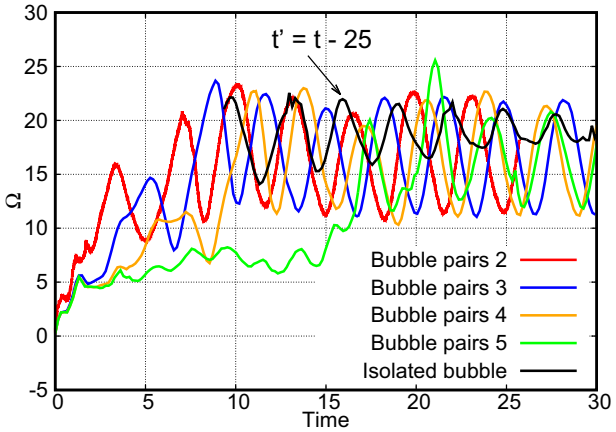

FIG. 24. Amount of ω_z accumulated at the bubble interface by changing the initial separated distance between the pair of bubbles, with respect to bubble pair 2−5 and the isolated bubble. It is observed that smaller S accelerate the accumulation of ω_z, and hence the critical Ω_{cri} for the onset of vortex shedding is reached earlier to trigger the repeated-bounce happening. In addition, although the isolated bubble rises in an spiral motion, the critical value of Ω to trigger the vortex shedding is identical to that of the bubble pair case.

shedding process is induced when the critical value of $\Omega \approx 22$ is reached [24]. Moreover, the vortex shedding frequencies among the four cases are almost identical, indicating that once the repeated bounce happens, the bubble motion is independent of the initially separated distance, with exactly the same zigzag motion. Although the isolated bubble shows spiral motion, we still observe the vortex to shed whenever the same critical value of $\Omega \approx 22$ is reached. Therefore, it is concluded that the maximum vortices to be accumulated at the bubble interface are dependent on the curvature of the bubble interface while it has little relevance to the type of the rising paths. Otherwise, we also notice that the oscillation of Ω for an isolated bubble is more stable over time ($t > 20$ or $t' > 45$) because of the gradually formed spiral motion, in which stage no vortex shedding happens [23,24].

Consequently, we find that the onset of the path instability of the bubble rising in flow type II is triggered earlier in the presence of another bubble, although this result is also observed in the experimental study [14] and the numerical investigation [26]. However, we indicate it is actually because the smaller separated distance accelerates the accumulation of the vorticities at the bubble interface, and hence the path instability happens earlier. From this point of view, the repeated-bounce behavior is actually a special type of zigzag motion, and it is not the real bounce interaction as the pair of bubbles rising within flow type I.

VI. EVOLUTION OF THE RISE VELOCITY AND THE EXPERIENCED FORCES

A. Evolution of the rise velocity for different bubble interactions

For the difference between the repeated-bounce and the attracting-bouncing motion, we have indicated that the former one is more like a noncontact zigzag motion while the latter one requires the pair of bubbles to collide with each other during the "kissing" period. As observed in experiments [14,32], the rise velocity drops sharply at the collision moment during the attracting-bouncing motion, while such decrease does not happen in the repeated-bouncing motion. Similarly, the evolution of the rise velocity for different bubble pairs are presented in Fig. 25, whereas the bouncing time is labeled with a dot-dashed vertical line.

As shown in the figure, the rise velocities of bubble pair 4 and bubble pair 14 are not affected at the bouncing moment and they just oscillate due to the zigzag motion. In contrast, in the cases of bubble pair 8 and bubble pair 12, which belong to the attracting-bounce motion, the rise velocities drop immediately at the bouncing moment and a loss of 10% is observed. Although it is still typically smaller than what is reported in experiment [14], however, we think it is related to the different fluid properties and different bouncing velocities, which actually determine the strength of the generated double-threaded vortex structures. The experiments also indicate that the repeated-bounce interactions are dominated by the wake instability rather than the bubble collision, and this is also in fully consistent with our aforementioned results that the repeated-bounce behavior is actually a particular case of the zigzag motion. Once it is triggered in the presence of another bubble, their dynamic behaviors are dominated by the periodically shedding vortices.

B. Experienced forces for different bubble interactions

The forces experienced by the rising bubble can be calculated by integrating the pressure and the viscous stresses applied by the liquid over the bubble interface [9,33] when body-fitted grids are adopted. However, the forces are difficult to compute accurately in the present framework, which uses an implicit VOF method. Although the interactions between the bubble and the surrounding liquid can be property tackled, nevertheless, it is still a challenge to estimate the forces at the bubble interface. The difficulty mainly lies in that the VOF method is a diffusive approach, and unlike the body-fitted method, the accuracy of the force interpolation at the interface is far from satisfactory. Correspondingly, some indirect methods are developed to calculate the forces experience by the unsteady moving droplet or bubble when the VOF method is applied [26,34]. Based on the Lagrangian framework proposed by Kok [4], the present study uses a theoretical model to describe the motion of a pair of bubbles interacting side by side in a viscous fluid with

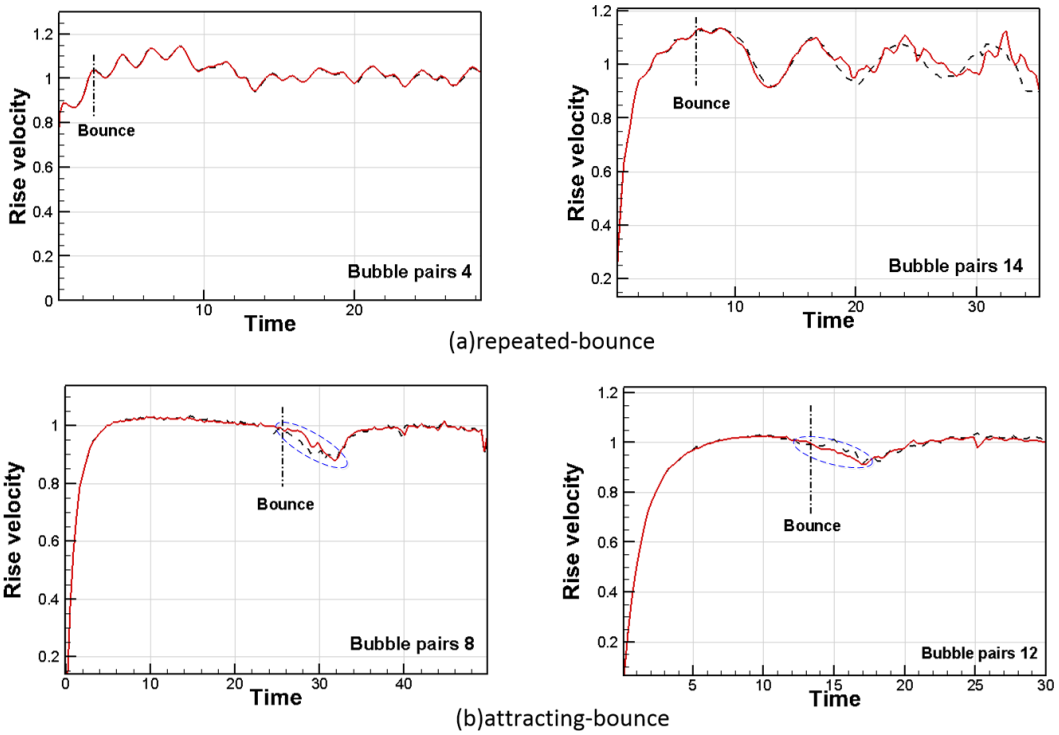

FIG. 25. Rise velocities for different bubble pairs. (a) Bubble pair 4 and bubble pair 14, corresponding to repeated-bounce motion; (b) bubble pair 8 and bubble pair 12, corresponding to attracting-bounce motion. Solid line: left bubble; dashed line: right bubble; dot-dashed vertical line: time instant for the bouncing moment. As shown in the dotted ellipse in panel (b), the rise velocity drops to almost 90% at collision; however, such decrease is not observed in panel (a).

high Reynolds number. In this model, the drag force experienced by the bubble is calculated from the viscous dissipation rate while the lift force is also estimated in a similar manner. After that, this model is used by De Vries *et al.* [35] to study a bubble bouncing on a vertical wall, and in order to include the vortical force rather than using the full potential flow approximation, the transverse force induced by the double-threaded vortices are estimated as $F_l = \pi \rho U_T^2 R/13$, which is obtained from the experimental data. However, it should be noted that such model is only applicable when the assumption of the spherical shape of bubbles holds true. Thereafter, Sanada *et al.* [14] extended it to model the bubble-bubble interactions and the results agree quite well with the experimental data when applying a correction coefficient to include the shape deformation. In their model, Kok's equations of bubble motion reduce to

$$\rho V \frac{dC_{Mz} w}{dt} = F_z, \tag{3}$$

$$\rho V \frac{dC_{Mx} u}{dt} = \frac{1}{4}\rho V \left[w^2 \frac{dC_{Mz}}{dx} + u^2 \frac{dC_{Mx}}{dx} \right] + F_x, \tag{4}$$

where C_{Mz} (C_{Mx}) is the added-mass coefficient corresponding to a bubble moving parallel (perpendicular) to a plane [36,37], and they are gived as

$$C_{Mz} = C_{M0}\left[1 + \frac{3}{16}\left(\frac{R}{x}\right)^3\right], \quad C_{Mx} = C_{M0}\left[1 + \frac{3}{8}\left(\frac{R}{x}\right)^3\right],$$

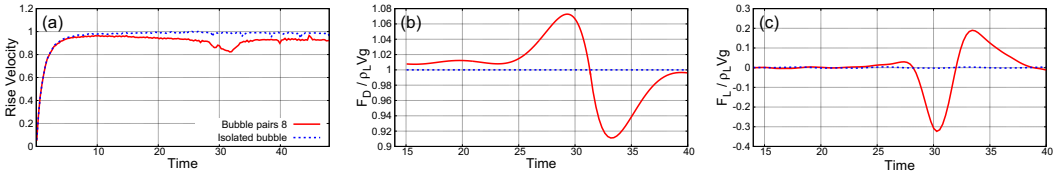

FIG. 26. (a) Rise velocity, (b) drag force, and (c) lift force for the left bubble in bubble pair 8 and for the isolated bubble. It is found that during the bubble collision, the rise velocity of the pair of bubbles drops as an indication of the drag enhancement. This is due to the increment of the shear rate inside the gap between the pair of bubbles that causes more vorticities to be produced at the bubble interface, as already shown in Fig. 12(b). For the evolution of F_L, it is observed that the lift force is repulsive during the bubbles collision; however, it becomes attractive gradually if the pair of bubbles are separated due to dissipation of the double-threaded vortices and the increase of the viscous force.

where C_{M0} is the added-mass coefficient for a bubble moving in an infinite flow domain, i.e., $C_{M0} = 0.5$ for a spherical bubble and $C_{M0} = \frac{(\chi^2-1)^{1/2}-\cos^{-1}\chi^{-1}}{\cos^{-1}\chi^{-1}-(\chi^2-1)^{1/2}\chi^{-2}}$ for an ellipsoidal bubble according to Lamb's theoretical study [38]. Note that in Kok's model, $F_z = \rho g V - D_z$ ($F_x = -D_x$) are the external forces directing vertically (transversely), where D_z (D_x) is the drag force due to viscous effect. As an improvement, De Vries *et al.* implemented the vortex force $F_{Lz} \sim \pi \rho u_T^2 R^2 \cos\beta$ ($F_{Lx} \sim \pi \rho u_T^2 R^2 \sin\beta$) into F_z (F_x) due to the double-threaded vortices where β is the inclination angle of the bubble short axis. Such implementation produces good results, as shown by Sanada *et al.* in their comparison with the experimental data even if their bubbles have significant deformations. In the present study, this model is also employed herein; however, we will not subdivide the drag (lift) force into different parts except for the added-mass force, which means the viscous force, the vortical force, and the history force are not dealt with explicitly but are implicit in the drag and lift. Therefore, these formulas are obtained:

$$F_D = \rho V \left(g - \frac{dC_{Mz} w}{dt} \right), \tag{5}$$

$$F_L = \rho V \left(\frac{dC_{Mx} u}{dt} - \frac{1}{4} \left[w^2 \frac{dC_{Mz}}{dx} + u^2 \frac{dC_{Mx}}{dx} \right] \right). \tag{6}$$

By substituting the velocities of the numerical results into Eqs. (5) and (6), we first discuss the force evolvement during the attracting-bounce interaction between a pair of bubbles, and case 8 is taken as an example. The rise velocities corresponding to the left bubble in bubble pair 8 and the isolated bubble are displayed in Fig. 26(a), and the drag force during collision is plotted in Fig. 26(b) by applying Eq. (5). After the acceleration stage, the isolated bubble almost rises with a constant velocity while bubble pair 8 shows a drop during the collision. This strongly suggests the drag force is increased significantly during the bubble collision, as validated in Fig. 26(b). Moreover, we should be aware that the drag increment has more to do with the viscous effects than with that of the capillary effects because the shear rate existing in the gap between the pair of bubbles is enhanced during the bubbles' approach, and this can be deduced by revisiting Fig. 12(b), which shows a sharp increment of vorticity level accumulated at the bubble interface during collision. The relationship between the drag force and the vorticity level has also been studied theoretically and numerically by Legendre [39], who indicates the drag force to be proportional to the maximum vorticities produced at the bubble interface, estimated as $F_D = -4 f(\chi, \mathrm{Re}) \pi \mu R^2 \omega_{\max}$ where $f(\chi, \mathrm{Re})$ is a function of the bubble deformation but only $f(\chi, \infty)$ and $f(\chi, 0)$ can be obtained as asymptotic solutions. Consequently, the increased shear rate inside the gap between the pair of bubbles induces more vorticities at the bubble surface and subsequently the drag force is enhanced. This result is also consistent with that of Takemura and Magnaudet [37], who study the bubble motion parallel to the

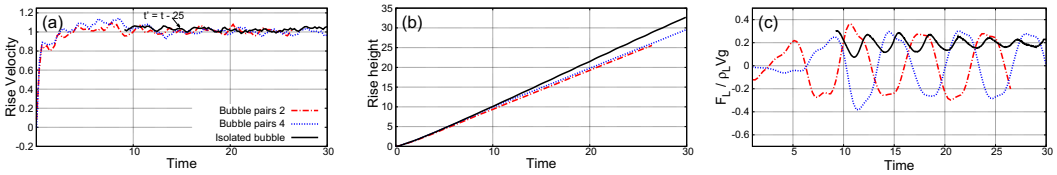

FIG. 27. (a) Rise velocity, (b) rise height, and (c) lift force for the left bubble in bubble pair 2 and bubble pair 4 and for the isolated bubble. It is found that with smaller separated distance, the pair of bubbles experience greater drag force and the bubble rises with lower velocity. For the lift force evolvement, the isolated spiralling bubble experiences a more steady lift force due to the spiral motion while different bubble pairs display the same oscillatory trend due to zigzag motion.

wall experimentally. They conclude that the essential repulsive effect from the vertical wall that induces the bouncing effect is actually the shear rate not the capillary effect. In the following stage after the pair of bubbles bounce off, the drag force decreases gradually due to the decline of the shear rate and the vorticity levels. Furthermore, we should also notice that even if the pair of bubbles rise in rectilinear paths after being separated, i.e., after $t > 35$, their rising velocities are still smaller than the isolated bubble, indicating the drag force coefficient ($C_D = F_D/0.5\rho u^2 \pi D^2$) within a bubble pair is still larger than that of an isolated bubble. This also agrees with results of Legendre and Magnaudet [9], who indicate the drag force coefficient is increased when spherical a pair of bubbles rise side by side because the interaction results in a higher strain rate in the fluid located between the two bubbles. Another aspect that deserves attention is the evolvement of the lift force during bubble collision as shown in Fig. 26(c). It is observed that F_L increases to a slightly positive value in the attracting stage, and subsequently when the bubbles get much closer, F_L declines sharply and finally becomes repulsive to repel the bubbles from one another due to the induced double-threaded vortices during the collision. In the following stage after the bubbles are separated, the repulsive force is decreased correspondingly because the viscous effects dominates gradually.

After that, we also calculate the forces experienced by the repeated-bounce within the bubble pair, while case 2 and case 4 are investigated to make the curves be more readable since the oscillatory motions are almost identical with other separated distances (cases 3 and 5). Rise velocities are shown in Fig. 27(a) and we do not observe noticeable differences between the pair of bubbles and the isolated bubble. However, if we compare the rising hight for different bubble pairs (isolated bubble) as shown in Fig. 27(b), it is more visible that smaller separated distance corresponding to slower rising height. Consequently, it is still identical with results of Legendre and Magnaudet [9] that a pair of bubbles experience greater drag force because of the strengthened shear rate inside the gap between the pair of bubbles. For the transverse oscillation, time histories of the lift force are shown in Fig. 27(c) that demonstrate the isolated spiralling bubble experiences a more steady lift force while different bubble pairs display the same oscillatory trend. Moreover, by comparing the transverse velocities of bubble pair 2 and bubble pair 4 in Fig. 22(a) with the lift forces in Fig. 27(c), it is clear that when the bubbles arrive at the furthermost or nearest position, i.e., $t = 11.8$, the lift force reaches the maximum absolute value due to the development of the shedding vortices, and at the corresponding moment, Ω is decreased to the minimum value as shown in Fig. 24.

VII. SUMMARY AND CONCLUSION REMARKS

A series of direct numerical simulations have been conducted to investigate the interactions between a pair of bubbles rising side by side. In contrast to the available experiments, this study aims to explore the in-depth physical mechanisms causing different interactions between the pair of bubbles, particularly focusing on the evolution of the vortex structures when repelling, attracting coalescence, attracting bounce, and repeated bounce are observed.

Fifteen bubble pairs are simulated in different silicon oils and we find the interactive behaviors between the pair of bubbles are actually related to the flow types generated by the bubble motion. If there are not toroidal vortex rings attached at the bubble rear, indicated by flow type I or transition A in the present study, the bubbles will attract with one another after being released in moderate- and high-Re flows, and thereafter, whether they will bounce or coalesce with one another after approaching is greatly dependent on the vortex developments. Even if an isolated bubble rises in a rectilinear path, the pair of bubbles may still bounce off when they attract one another. By applying an available model to calculate the drag forces and the lift forces experienced by the pair of bubbles, the mechanism to produce the bouncing behavior is ascribed to the increased shear rate inside the gap between the pair of bubbles which acts to enhance the viscous effects as more vorticities are introduced at the bubble interface. Under such a case, the drag force which is proportional to the maximum vorticity at the bubble interface is also increased accordingly. Meanwhile, the lift force to repel the pair of bubbles is also produced during the collision because of the generated double-threaded wake due to the strengthened vorticity level and thereafter the pair of bubbles bounce off after the "kissing" period. Furthermore, we also explain why the interaction between the pair of bubbles will evolve from attracting coalescence to attracting bounce by either increasing the bubble size or widening the separated distances, which is because the double-threaded wake vortices are more likely to be born if the bubble shape is more flat and the developing time is longer.

In contrast, if there are toroidal vortex rings generated in the bubble wake, indicated by flow type II or transition B in the present study, the pair of bubbles will always repel one another after being released. This is because the inner eddies will be squeezed due to the increased shear inside the gap between the pair of bubbles and thereafter the axisymmetric structure of the vortex rings is destroyed and the lift force is induced. However, whether they will repel forever or show a repeated-bounce motion is dependent on the the rising behavior of the isolated bubble and the fluid properties. A smaller separated distance favors triggering the repeated bounce earlier because the shear rates inside the gap between the pair of bubbles are greater. Moreover, we find even if the isolated bubble shows a spiral motion, it will be restricted to rise in a zigzag manner when another bubble is placed side by side. Detailed studies about ω_z accumulated on the bubble interface and the tracking of the force further indicate the repeated-bounce motion to be a particular type of zigzag motion where once the symmetry is broken the behaviors of the repeated bounce have nothing to do with the separated distances.

One piece of information available from the numerical results reported in this paper is that, for bubble interactions inside the bubbly flow, the double-threaded vorticity-induced effect is very important and the wake interactions can produce more flow agitation in the bulk liquid. Thus, it would be helpful to explain why the horizontal clustering predicted by the irrotational flow model is not observed in experiments. Besides, since most of the direct numerical simulations [40–42] just consider the nearly spherical or small deformed bubbly flows, the three-dimensional vorticity effect should play a more important role in the dynamics of bubbly suspensions in which the wake-induced bouncing preventing clustering are generated.

ACKNOWLEDGMENTS

The authors gratefully acknowledge the support from the NSFC (No. 51636009, No. 11872296, and No. U1732276) and CAS (No. XDB22040201 and No. QYZDJ-SSW-SLH014). J.Z. gratefully acknowledges the Young Elite Scientists Sponsorship Program by YESS (No. 2018QNRC001).

[1] P. Smereka, On the motion of bubbles in a periodic box, J. Fluid Mech. **254**, 79 (1993).

[2] A. S. Sangani and A. K. Didwania, Dynamic simulations of flows of bubbly liquids at large Reynolds numbers, J. Fluid Mech. **250**, 307 (1993).

[3] J. H. Lammers and A. Biesheuvel, Concentration waves and the instability of bubbly flows, J. Fluid Mech. **328**, 67 (1996).
[4] J. B. W. Kok, Dynamics of a pair of gas bubbles moving through liquid. I: Theory, Eur. J. Mech. B **12**, 515 (1993).
[5] J. F. Harper, On bubbles rising in line at large Reynolds numbers, J. Fluid Mech. **41**, 751 (1970).
[6] H. Yuan and A. Prosperetti, On the in-line motion of two spherical bubbles in a viscous fluid, J. Fluid Mech. **278**, 325 (1994).
[7] J. F. Harper, Bubbles rising in line: Why is the first approximation so bad? J. Fluid Mech. **351**, 289 (1997).
[8] T. Sanada, M. Watanabe, and T. Fukano, Interaction and coalescence of bubbles in stagnant liquid, Multiphase Sci. Technol. **18**, 155 (2006).
[9] D. Legendre, J. Magnaudet, and G. Mougin, Hydrodynamic interactions between two spherical bubbles rising side by side in a viscous liquid, J. Fluid Mech. **497**, 133 (2003).
[10] Y. Hallez and D. Legendre, Interaction between two spherical bubbles rising in a viscous liquid, J. Fluid Mech. **673**, 406 (2011).
[11] J. Magnaudet and G. Mougin, Wake instability of a fixed spheroidal bubble, J. Fluid Mech. **572**, 311 (2007).
[12] J. C. Cano-Lozano, P. Bohorquez, and C. Martínez-Bazán, Wake instability of a fixed axisymmetric bubble of realistic shape, Int. J. Multiphase Flow **51**, 11 (2013).
[13] P. C. Duineveld, Bouncing and coalescence of bubble pairs rising at high Reynolds number in pure water or aqueous surfactant solutions, *Fascination of Fluid Dynamics* (Springer, Dordrecht, 1998), pp. 409–439.
[14] T. Sanada, A. Sato, M. Shirota, and M. Watanabe, Motion and coalescence of a pair of bubbles rising side by side, Chem. Eng. Sci. **64**, 2659 (2009).
[15] P. C. Duineveld, The rise velocity and shape of bubbles in pure water at high Reynolds number, J. Fluid Mech. **292**, 325 (1995).
[16] J. Magnaudet and I. Eames, The motion of high-Reynolds-number bubbles in inhomogeneous flows, Annu. Rev. Fluid Mech. **32**, 659 (2000).
[17] K. Lunde and R. Perkins, Observations on wakes behind spheroidal bubbles and particles, in *Proceedings of the ASME Fluids Engineering Division Summer Meeting, Vancouver, Canada* (ASME, New York, 1997), Paper 97–3530.
[18] K. Ellingsen and F. Risso, On the rise of an ellipsoidal bubble in water: Oscillatory paths and liquid-induced velocity, J. Fluid Mech. **440**, 235 (2001).
[19] C. Brücker, Structure and dynamics of the wake of bubbles and its relevance for bubble interaction, Phys. Fluids **11**, 1781 (1999).
[20] G. Mougin and J. Magnaudet, Path Instability of a Rising Bubble, Phys. Rev. Lett. **88**, 014502 (2001).
[21] W. L. Shew, S. Poncet, and J.-F. Pinton, Force measurements on rising bubbles, J. Fluid Mech. **569**, 51 (2006).
[22] B. Yang and A. Prosperetti, Linear stability of the flow past a spheroidal bubble, J. Fluid Mech. **582**, 53 (2007).
[23] J. C. Cano-Lozano, C. Martinez-Bazan, J. Magnaudet, and J. Tchoufag, Paths and wakes of deformable nearly spheroidal rising bubbles close to the transition to path instability, Phys. Rev. Fluids **1**, 053604 (2016).
[24] J. Zhang and M.-J. Ni, What happens to the vortex structures when the rising bubble transits from zigzag to spiral? J. Fluid Mech. **828**, 353 (2017).
[25] S. Popinet, An accurate adaptive solver for surface-tension-driven interfacial flows, J. Comput. Phys. **228**, 5838 (2009).
[26] M. K. Tripathi, A. R. Premlata, K. C. Sahu, and R. Govindarajan, Two initially spherical bubbles rising in quiescent liquid, Phys. Rev. Fluids **2**, 073601 (2017).
[27] M. K. Tripathi, K. C. Sahu, and R. Govindarajan, Dynamics of an initially spherical bubble rising in quiescent liquid, Nat. Commun. **6** (2015).
[28] X. Chen and V. Yang, Thickness-based adaptive mesh refinement methods for multi-phase flow simulations with thin regions, J. Comput. Phys. **269**, 22 (2014).

[29] R. Zenit and J. Magnaudet, Path instability of rising spheroidal air bubbles: A shape-controlled process, Phys. Fluids **20**, 061702 (2008).
[30] M. C. Thompson, T. Leweke, and M. Provansal, Kinematics and dynamics of sphere wake transition, J. Fluids Struct. **15**, 575 (2001).
[31] L. Zeng, S. Balachandar, and P. Fischer, Wall-induced forces on a rigid sphere at finite Reynolds number, J. Fluid Mech. **536**, 1 (2005).
[32] E. Yamaguchi and T. Sanada, Bouncing of a pair of clean bubbles rising side by side, in *The Ninth JSME-KSME Thermal and Fluids Engineering Conference, October 27–30, 2017, Okinawa, Japan* (2017).
[33] A. Blanco and J. Magnaudet, The structure of the axisymmetric high-Reynolds-number flow around an ellipsoidal bubble of fixed shape, Phys. Fluids **7**, 1265 (1995).
[34] X. Chen, C. Xue, L. Zhang, G. Hu, X. Jiang, and J. Sun, Inertial migration of deformable droplets in a microchannel, Phys. Fluids **26**, 112003 (2014).
[35] A. W. G. De Vries, A. Biesheuvel, and L. Van Wijngaarden, Notes on the path and wake of a gas bubble rising in pure water, Int. J. Multiphase Flow **28**, 1823 (2002).
[36] L. M. Milne-Thomson, *Theoretical Hydrodynamics*, 5th ed. (Dover, New York, 1996), Vol. 8.
[37] F. Takemura and J. Magnaudet, The transverse force on clean and contaminated bubbles rising near a vertical wall at moderate Reynolds number, J. Fluid Mech. **495**, 235 (2003).
[38] H. Lamb, *Hydrodynamics* (Cambridge University Press, Cambridge, UK, 1993).
[39] D. Legendre, On the relation between the drag and the vorticity produced on a clean bubble, Phys. Fluids **19**, 018102 (2007).
[40] B. Bunner and G. Tryggvason, Dynamics of homogeneous bubbly flows, Part 1. Rise velocity and microstructure of the bubbles, J. Fluid Mech. **466**, 17 (2002).
[41] B. Bunner and G. Tryggvason, Effect of bubble deformation on the properties of bubbly flows, J. Fluid Mech. **495**, 77 (2003).
[42] A. Loisy, A. Naso, and P. D. M. Spelt, Buoyancy-driven bubbly flows: Ordered and free rise at small and intermediate volume fraction, J. Fluid Mech. **816**, 94 (2017).